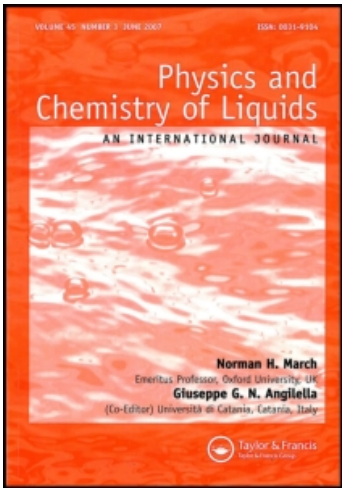

Physics and Chemistry of Liquids
Publication details, including instructions for authors and subscription information:
http://www.informaworld.com/smpp/title~content=t713646857

Determination of Three Body Correlations in Simple Liquids by RMC Modelling of Diffraction Data. II. Elemental Liquids

M. A. Howe[ab]; R. L. McGreevy[ac]; L. Pusztai[d]; I. Borzsák[d]
[a] Department of Physics, Oxford University, Clarendon Laboratory, Oxford, UK [b] Institute of Hydrology, Wallingford, Oxon, UK [c] Studsvik Neutron Research Laboratory, Nyköping, Sweden [d] Laboratory of Theoretical Chemistry, L. Eötvös University, Budapest 112, Hungary

To cite this Article Howe, M. A. , McGreevy, R. L. , Pusztai, L. and Borzsák, I.(1993) 'Determination of Three Body Correlations in Simple Liquids by RMC Modelling of Diffraction Data. II. Elemental Liquids', Physics and Chemistry of Liquids, 25: 4, 205 — 241
To link to this Article: DOI: 10.1080/00319109308030363
URL: http://dx.doi.org/10.1080/00319109308030363

Phys. Chem. Liq., 1993, Vol. 25, pp. 205–241
Reprints available directly from the publisher
Photocopying permitted by license only

DETERMINATION OF THREE BODY CORRELATIONS IN SIMPLE LIQUIDS BY RMC MODELLING OF DIFFRACTION DATA. II. ELEMENTAL LIQUIDS

M. A. HOWE* and R. L. MCGREEVY†

Department of Physics, Oxford University, Clarendon Laboratory, Parks Road, Oxford, OX1 3PU, UK

L. PUSZTAI and I. BORZSÁK

Laboratory of Theoretical Chemistry, L. Eötvös University, Budapest 112, Pf. 32, H-1518 Hungary

(Received 3 July 1992)

The structures of 51 elemental liquids have been modelled from experimental diffraction data using the reverse Monte Carlo method. The structural trends across the periodic table are described in terms of three-body correlations and discussed in terms of the relative importance of two-body and many-body forces.

KEY WORDS: Reverse Monte Carlo method, many-body forces.

1 INTRODUCTION

In the first part of this review[1] we describe the Reverse Monte Carlo[2] (RMC) method of obtaining model structures of disordered systems based on the structure factors obtained by experiment. We then went on to present the results of some tests of the method in which we used the structure factors obtained from Monte Carlo (MC) simulations and determined to what extent an RMC calculation would reproduce the three-body correlations of the simulation. We concluded that RMC does indeed work successfully if the potentials are pairwise additive. In cases where they are not then the imposition of constraints, e.g. modelling molecular systems with molecules rather than atoms, can enable the three dimensional structure to be determined. We also concluded that when the potentials are very complex, which usually makes the problem difficult for MC or molecular dynamics (MD) simulations, RMC with constraints is still a valuable way of distinguishing between various structural possibilities.

* *Current address*: Institute of Hydrology, Crowmarsh Gifford, Wallingford, Oxon OX10 8BB, UK.
† *Current address*: Studsvik Neutron Research Laboratory, S-611 82 Nyköping, Sweden.

In this second part we present the results of RMC calculations for a large number of elemental liquids (See Table 1 and Figure 1). Many of these liquids can be well described by pairwise additive potentials so we expect the application of RMC to be straightforward and to accurately reproduce the three body correlations. In other cases, however, there is more of a molecular nature to the liquid which means that three-body interactions are not negligible and simple RMC does not necessarily produce the right structure. Here the use of coordination constraints has allowed us to explore the variety of structures that are consistent with the experimentally determined structure factors.

2 THE METHOD

Details of the RMC method have been given before[1,2] so we shall just give a brief summary. The aim is to produce three dimensional structural models of a system that are consistent with the available diffraction data, within the errors of that data. To do this we use a modification of the standard Metropolis Monte Carlo (MMC) method[3] where, instead of minimising the system energy, we minimise the difference between the calculated and experimental spectra. The algorithm is as follows.

1) Start with an initial configuration, i.e. a set of coordinates in a box representing atomic positions, with periodic boundary conditions. Calculate the radial distribution function

$$g_{\mathrm{rmc}}(r) = \frac{n_{\mathrm{rmc}}(r)}{4\pi r^2 \rho \Delta r} \tag{1}$$

where ρ is the atomic number density and $n_{\mathrm{rmc}}(r)$ is the number of atoms at a distance between r and $r + \Delta r$ from a central atom, averaged over all atoms as centres. Transform to the structure factor

$$S_{\mathrm{rmc}}(Q) = 1 + \rho \int_0^\infty 4\pi r^2 (g_{\mathrm{rmc}}(r) - 1) \frac{\sin Qr}{Qr} \, \mathrm{d}r \tag{2}$$

and calculate

$$\chi^2 = \sum_i [S_{\mathrm{rmc}}(Q_i) - S_{\mathrm{expt}}(Q_i)]^2 / \sigma^2(Q_i) \tag{3}$$

where $S_{\mathrm{expt}}(Q_i)$ is the experimentally measured structure factor and $\sigma(Q_i)$ is a measure of the experimental error.

2) Move one atom at random. Calculate the new $g_{\mathrm{rmc}}(r)$, $S_{\mathrm{rmc}}(Q)$ and thus the new χ^2, let us call it χ'^2.

3) If $\chi'^2 < \chi^2$ the move is accepted. If $\chi'^2 > \chi^2$ the move is accepted with probability $\exp(-(\chi'^2 - \chi^2)/2)$, otherwise it is rejected.

4) Repeat from step 2.

χ^2 will initially decrease until it reaches an equilibrium value about which it will oscillate. The resulting configuration should be a three dimensional structure that is consistent with the experimental structure factor within the experimental error. Further independent configurations may then be collected by continuing to run the simulation under the same conditions as for MMC.

This algorithm is usually modified slightly by the imposition of a minimum 'hard sphere' radius for atoms. This helps to compensate for some errors in the experimental data and avoids atoms coming unphysically close together. For some of the elemental liquids we have also used a coordination constraint in several ways. The method is as follows. Calculate the coordination number, i.e. the number of atoms within a certain distance, r_c, of every atom and thus the fraction f_{rmc} of atoms in the configuration that have the required coordination number. Then add on to χ^2 an additional term, χ_c^2, given by

$$\chi_c^2 = (f_{\text{rmc}} - f_{\text{req}})^2/\sigma_c^2, \tag{4}$$

where f_{req} is the required fraction and σ_c is effectively a weighting factor of the coordination constraint relative to the structure factor constraint. We can maximise the number of atoms with a certain coordination number by putting $f_{\text{req}} = 1$. If we choose a starting configuration for which $f_{\text{req}} = 1$ and a very small value for σ_c any change in f_{rmc} would cause a very large change in χ_c^2 with negligible chance of being accepted. This effectively prevents 'bonds' from being broken and allows us to create a model with a particular type of molecular unit, or keep the 'bonding' in molecular units that already exist. However, because there are no angular constraints, such molecules are not rigid. Rigid molecules can be introduced specifically; the random motion of a particle is then replaced by a random translation and rotation of the molecule[5].

3 RESULTS OF RMC CALCULATIONS ON ELEMENTAL LIQUIDS

Structure factors, obtained by neutron and X-ray scattering, are reported in the literature for many of the elements. In some cases they are published as tabulated values and in other cases the tabulated data was obtainable from the authors. For the remaining data the published graphs had to be converted into numerical form; this was achieved using a digitising tablet. The resulting structure factor data was then plotted to make sure that it accurately reproduced the original graphs.

Table 1 lists all the structure factor data for which results are described here. The elements are also shown on the periodic table in Figure 1. The results for liquid nitrogen and the halogens[5] and some of the results for molten caesium[6] and helium-4[7] have appeared elsewhere; the remainder have not previously been published. We expect to publish more detailed results for phosphorus and sulphur separately.

For some elements more than one set of data was available. It was sometimes clear that one of these sets was preferable to another because, for example, it covered a larger region of Q-space, was less noisy, or its Fourier transform to $g(r)$ was better behaved in the small r region. These methods of data assessment are described further

Table 1 Details of data sets modelled

Element	*Atomic number*	*Group*	*Method*	*Temperature (°C)*	*Density (Å^{-3})*	*References*
Al	13	IIb	neutron	680	0.0526	t1
Ar	18	0	neutron	−188	0.02125	t2
As	33	Vb	neutron	825	0.0419	t3
Au	79	Ib	neutron	1100	0.0528	t4
Bi	83	Vb	neutron	293	0.0289	t5
Br	35	VIIb	x-ray	20	0.02352	t6
Ce	58	L	x-ray	870	0.0287	t19
Cl	17	VIIb	neutron	22	0.02384	t7
Co	27	VIII	x-ray	1515	0.0781	t8
Cs	55	Ia	neutron	30	0.00832	t9, t22
			neutron	50	0.00829	t10
			neutron	300	0.00761	t10
			neutron	500	0.00698	t10
			neutron	600	0.00684	t40
			neutron	700	0.00657	t10
			neutron	900	0.00603	t10
			neutron	1100	0.00548	t10
			neutron	1400	0.00434	t10
			neutron	1650	0.00267	t10
Cu	29	Ib	neutron	1120	0.0750	t11
			neutron	1560	0.072	t11
Dy	66	L	x-ray	1430	0.0302	t12
Er	68	L	x-ray	1520	0.0301	t12
Eu	63	L	x-ray	830	0.0183	t19
F	9	VIIb	neutron	−196	0.0495	t13
Fe	26	VIII	x-ray	1550	0.0755	t8
Ga	31	IIIb	neutron/ x-ray	20	0.05272	t14
Gd	64	L	x-ray	1330	0.0265	t19
Ge	32	IVb	neutron	1000	0.0456	t15
			x-ray	980	0.0456	t16
He	2	0	x-ray	−270	0.0226	t17
Hg	80	IIb	x-ray	20	0.04068	t18
Ho	67	L	x-ray	1480	0.0301	t12
I	53	VIIb	x-ray	120	0.0185	t20
In	49	IIIb	x-ray	166	0.0368	t21
K	19	Ia	neutron	65	0.0127	t9, t22
Kr	36	0	neutron	−156	0.0176	t23
			neutron	−73	0.01206	t24
			neutron	−73	0.01102	t24
La	57	IIIa	x-ray	970	0.0258	t19
Li	3	Ia	neutron	197	0.0445	t25, t22
			x-ray	191	0.0445	t25, t22
N	7	Vb	neutron	−208	0.03702	t26
Na	11	Ia	x-ray	100	0.0243	t27
Nd	60	L	x-ray	1050	0.0289	t12
Ne	10	0	neutron	−247	0.0358	t28
			neutron	−238	0.0347	t29
			neutron	−238	0.0317	t29
Ni	28	VIII	x-ray	1475	0.0796	t8
P	15	Vb	neutron	10	0.03455	t30, t31
			neutron	50	0.03384	t30, t31
Pb	82	IVb	neutron	340	0.03093	t32
Pd	46	VIII	x-ray	1580	0.0594	t33

Table 1 *Continued*

Element	*Atomic number*	*Group*	*Method*	*Temperature (°C)*	*Density (Å^{-3})*	*References*
Pr	59	L	x-ray	950	0.0282	t19
Pt	78	VIII	x-ray	1780	0.0577	t33
Rb	37	Ia	neutron	40	0.0103	t34
S	16	VIb	neutron	130	0.0335	t35
			neutron	220	0.0330	t35
Sb	51	Vb	neutron	658	0.0322	t36
			neutron	660	0.0322	t37
Sc	21	IIIa	x-ray	1560	0.0391	t19
Se	34	VIb	neutron	265	0.0298	t39
Si	14	IVb	x-ray	1460	0.0538	t16
Sn	50	IVb	neutron	250	0.0345	t43
Tb	65	L	x-ray	1380	0.0274	t19
Te	52	VIb	neutron	450	0.0272	t44, t45
			neutron	460	0.0272	t46, t45
Tl	81	IIIb	neutron	315	0.0331	t48, t49
Yb	70	L	x- ray	850	0.0216	t19
Zn	30	IIb	neutron	450	0.0604	t50
			x-ray	450	0.0604	t50
Zr	40	IVa	x-ray	1900	0.0391	t33

elsewhere[4]. Otherwise we performed independent RMC calculations for the different data sets and compared them.

In all cases we used configurations of between 3000 and 4096 atoms. In most cases the starting configuration was created by placing atoms in the configuration box at random positions and then moving them until the constraint on closest distance of approach of atoms was satisfied. The exceptions to this were some of the molecular

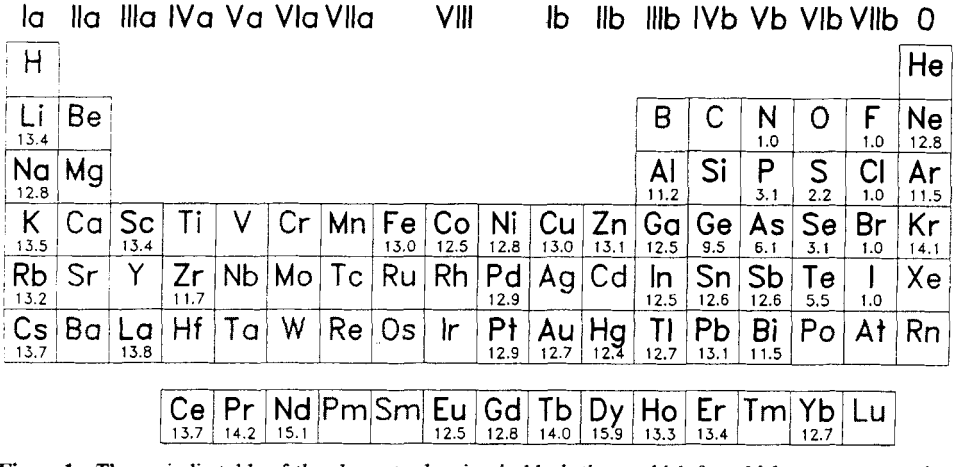

Figure 1 The periodic table of the elements showing in black those which for which we are presenting the results of RMC calculations. Values of $\langle n_{si} \rangle$ are given.

Table 2 Some parameters for the simple liquids

Element	*Temperature* (°C)	*Density* ($Å^{-3}$)	Q_1 ($Å^{-1}$)	ρ/Q_1^3 (10^{-3})	r_1 (Å)	$Q_1 r_1$	r_c (Å)	$\langle n_c \rangle$
Al	680	0.0526	2.65	2.82	2.8	7.4	3.7	11.2
Ar	−188	0.02125	2.026	2.56	3.7	7.5	5.1	11.5
Au	1100	0.0528	2.70	2.68	2.8	7.6	3.9	12.7
Ce	870	0.0287	2.10	3.10	3.3	6.9	4.9	13.7
Co	1515	0.0781	3.00	2.89	2.5	7.5	3.4	12.5
Cs	30	0.00832	1.40	3.03	5.4	7.6	7.4	13.7
Cu	1120	0.0750	3.0	2.78	2.5	7.5	3.5	13.0
Dy	1430	0.0302	2.1	3.26	3.5	7.4	5.1	15.9
Er	1520	0.0301	2.2	2.82	3.4	7.5	4.8	13.4
Eu	830	0.0183	1.90	2.67	3.8	7.2	5.5	12.5
Fe	1550	0.0755	3.0	2.79	2.5	7.5	3.5	13.0
Gd	1330	0.0265	2.10	2.86	3.5	7.4	4.9	12.8
Ho	1480	0.0301	2.25	2.65	3.4	7.7	4.8	13.3
K	65	0.0127	1.65	2.82	4.6	7.6	6.4	13.5
Kr	−156	0.0176	1.80	3.02	3.9	7.0	5.9	14.1
La	970	0.0258	2.15	2.60	3.5	7.5	5.1	13.8
Li	197	0.0445	2.5	2.85	3.0	7.5	4.2	13.4
Na	100	0.0243	2.04	2.87	3.7	7.6	5.0	12.8
Nd	1050	0.0289	2.1	3.13	3.4	7.1	5.1	15.1
Ne	−246	0.0358	2.40	2.59	3.1	7.4	4.5	12.8
Ni	1475	0.0796	3.1	2.67	2.4	7.4	3.4	12.8
Pb	340	0.03093	2.198	2.92	3.3	7.3	4.7	13.1
Pd	1580	0.0594	2.8	2.70	2.6	7.3	3.8	12.9
Pr	950	0.0282	2.10	3.05	3.4	7.1	5.0	14.2
Pt	1780	0.0577	2.75	2.78	2.6	7.2	3.8	12.9
Rb	40	0.0103	1.5	3.05	4.8	7.2	6.8	13.2
Sc	1560	0.0391	2.40	2.83	2.8	6.7	4.4	13.4
Tb	1380	0.0274	2.10	2.96	3.5	7.4	5.0	14.0
Tl	315	0.0331	2.25	2.91	3.2	7.2	4.5	12.7
Yb	850	0.0216	1.95	2.91	3.8	7.4	5.3	12.7
Zn	450	0.0604	2.85	2.61	2.7	7.7	3.8	13.1
Zr	1900	0.0391	2.35	3.01	3.1	7.3	4.1	11.7

systems described later. The RMC calculation was then run until a good fit to the experimental data was achieved. The general approach we adopted was to perform an RMC calculation with no coordination constraints and then investigate the local structure within the distance defined by the first minimum in $g(r)$. In the cases where it was appropriate we then went on to investigate alternative structures obtainable using coordination constraints.

The structure factor of most of the elemental liquids are very similar. They are liquids that can be described well using pairwise additive potentials and have a relatively simple structure. We shall consider these 'simple' liquids first and then go on to consider the remaining 'complex' liquids.

3.1 *Simple liquids*

Because of the differing sizes of the atoms in the various liquids the structure factors of the elements would be expected to peak at different Q values. It is therefore better

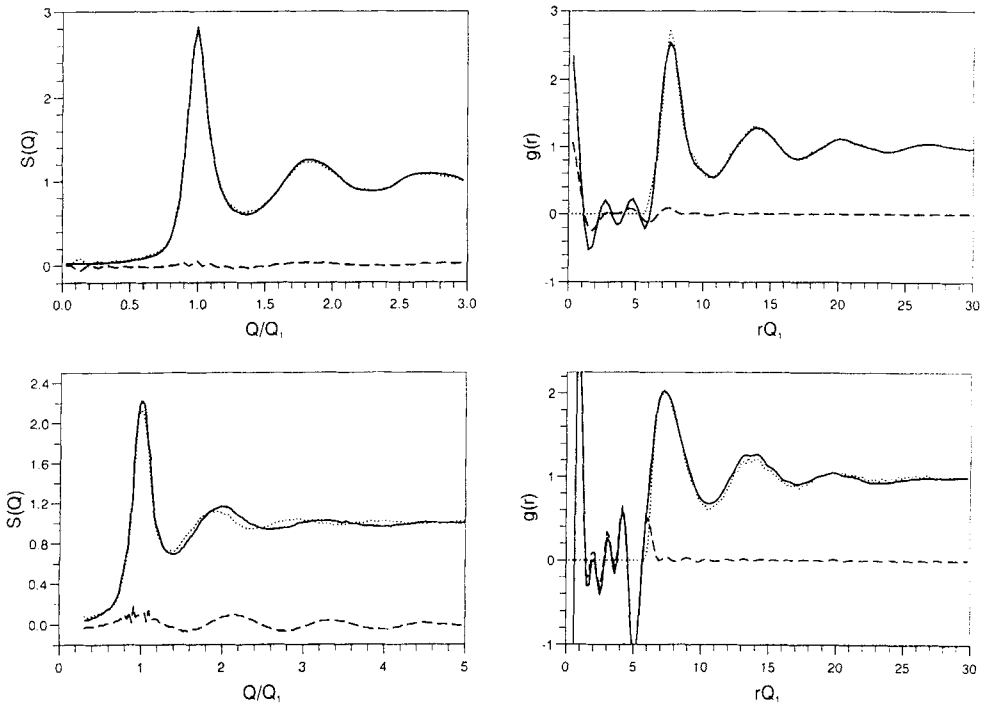

Figure 2 Examples of RMC fits for the simple liquids: top copper, bottom europium. On the left we show the experimental structure factor (solid line), the RMC fit to it (dotted line), and the difference (dashed line); on the right we show the $g(r)$ obtained by Fourier transformation of the experimental data (solid line), that obtained from RMC (dotted line), and the difference (dashed line).

to compare them when plotted as a function of some dimensionless variable such as Q/Q_1, where Q_1 is the position of the first peak in $S(Q)$. When this is done the structure factors for 32 of the elements are found to be very similar whilst those of the remainder are significantly different. We shall call the former simple liquids; they are listed in Table 2.

Because of space considerations we cannot show all the fits but two examples are given in Figure 2. In most cases the RMC calculations produced a good fit to the experimental structure factor with the case of molten copper, shown in the figure, being a typical example. However in some cases, namely those of dysprosium, erbium, europium, holmium, neodynium, scandium and terbium[12,19] it was not possible to fit the structure factor well. The example of europium is also shown in figure 2 where it can be seen that on Fourier transformation to real space the experimentally determined $g(r)$ is fitted well except in the region where r is less than the closest distance of approach allowed. This means that it is not possible to fit the structure factor well with a physically reasonable structure and therefore that the experimental data in these cases must contain significant errors. Nonetheless, the fits we do obtain are consistent with these being simple liquids so we have included the results in Table 2 even though they may be less accurate than the remainder.

The details of the experimental data and RMC fits are given in Table 2. For those elements for which we have more than one set of data we have used that corresponding to the highest density. Densities have been expressed in a dimensionless form by dividing Q_1^3; they vary from 2.56 to 3.13. We also give values of r_1, the position of the first maximum in $g(r)$, r_c, the position of the first minimum in $g(r)$, the product Q_1, r_1, and the average coordination number, $\langle n_c \rangle$, which is the average number of atoms within a distance r_c from a central atom. The structure factor data is defined typically at 0.05 Å^{-1} to 0.1 Å^{-1} intervals whilst the pair correlation function $g(r)$ is calculated at 0.1 Å intervals and this determines the precision of Q_1, r_1, r_c, and the quantities derived from them. The resulting uncertainty in $Q_1 r_1$ is approximately ± 0.3; within this margin of error $Q_1 r_1$ can be considered to be constant with a mean value of 7.4.

The value of $\langle n_c \rangle$ depends quite critically on the value of r_c. For example, for aluminium increasing r_c from 3.7 to 3.8 Å increases $\langle n_c \rangle$ from 11.2 to 11.8. As in some cases there is some ambiguity in determining the value of r_c even to the nearest 0.1 Å, it is clear that the quoted coordination numbers should not be considered particularly precise (coordination numbers are often quoted for such liquids with an unrealistic precision). We can see, though, that they are consistent with one another, varying from 11 to 15, with a mean value of 13.2. There is also some correlation between density and coordination number, with coordination number increasing with density, as would be expected. This is shown in the case of copper by fitting the higher temperature data, for which the density is lower, where we obtain $\langle n_c \rangle = 12.6$ rather than 13.0.

The details we have discussed so far are all obtainable directly from $S(Q)$ and from $g(r)$, which can be obtained from $S(Q)$ by Fourier transformation. It might be thought, therefore, that we have not gained anything by using RMC. This is in fact not entirely true as RMC has produced self-consistent structures and in so doing allows us to overcome, to some extent, certain systematic errors in the data. However with the RMC model we can go on to consider three-particle correlations such as 'bond-angle' distributions.

In Figure 3 we show the structure factors, $S(Q/Q_1)$, the pair correlation functions, $g(rQ_1)$, and the bond-angle correlations, $b(\cos\theta)$, for the simple liquids. $b(\cos\theta)$ is defined as the probability of two neighbours within r_c of a central atom forming an angle θ with the central atom. We see that the structure factors are very similar. In fact the only significant difference is in the sharpness of the first peak; this is indicative of the range of structural correlations. The $g(r)$'s are also similar, with the main difference again being the height of the first peak. Looking at the bond-angle correlations we see that argon, which has the lowest reduced density of all the liquids, has a slightly higher peak than the rest, otherwise they are all quite similar with some variation in the height of the mean peak coupled with a shift from $\cos\theta \approx 0.58$ ($\theta \approx 54.5°$) to $\cos\theta \approx 0.65$ ($\theta \approx 49.5°$). Given the similarity in structure factors it is hardly surprising that the structures produced by RMC have almost identical three body correlations. Analysis of the bond angle distributions using the method of spherical harmonic invariants[8] shows that the local structure of these liquids may be described as a distortion of the hexagonal close packed (hcp) structure. This is

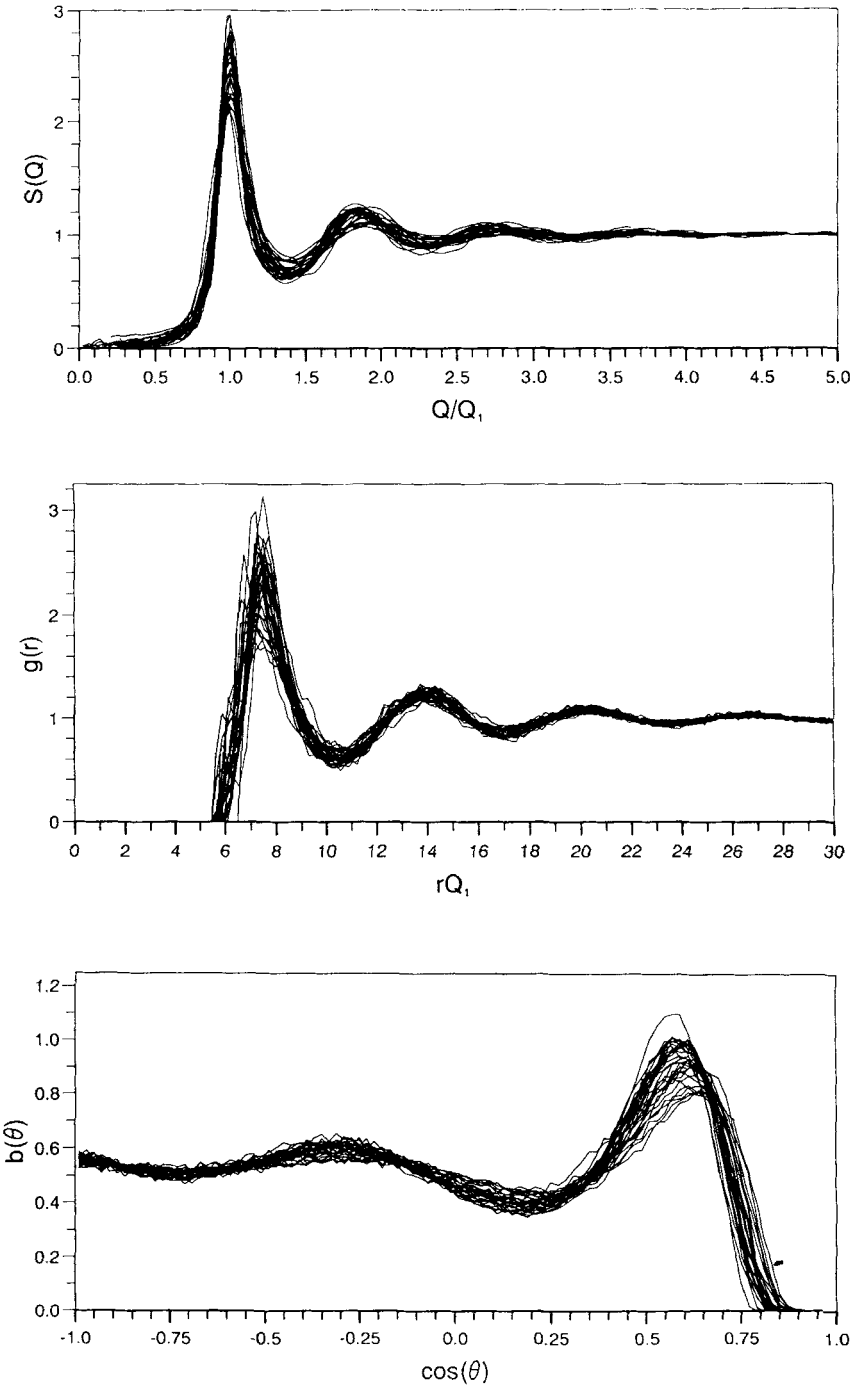

Figure 3 RMC results for the 'simple liquids'. Top: $S(Q)$. Middle: $g(r)$. Bottom: $b(\theta)$.

consistent with the average coordination numbers. The alkali metals, europium, iron and zirconium melt from a body-centred cubic crystal structure but the remainder melt from a close-packed structure, hexagonal in the case of many of the transition metals and cubic in the remainder.

All the results discussed so far were obtained at densities close to the triple point densities. It is to be expected that there will be a change in structure as the temperature is increased and density decreased. We have reported elsewhere[6] the results of RMC modelling of molten caesium at various points along the liquid-vapour co-existence curve. As the temperature is increased from 50°C, through 300°C, 500°C, 700°C, 900°C, 1100°C, and 1400°C to 1650°C the positions of the first maximum and first minimum of the radial distribution function remain approximately constant, with values of $r_1 \approx 5.5$ Å and $r_c \approx 7.5$ Å (although r_c has the slightly higher value of 7.8 Å at the highest temperature). This means that one can still think of there being a first coordination shell within this distance. The mean coordination number decreases linearly with density but the spread in coordination numbers of individual atoms broadens considerably indicating a tendency to cluster at the lower densities. An analysis using spherical harmonic invariants suggests that the local structure changes from hexagonal close packed through body-centred cubic to icosahedral at 1100°C. The lower densities of krypton and neon also show icosahedral local symmetry but the level of disorder is, of course, greater than that at the higher densities.

It should be stressed at this stage that description of the local structure in terms of a crystalline 'analogue' is made on the basis of the average bond orientational order within the first coordination shell only, in comparison to a restricted set of possible crystalline symmetries. One should not therefore interpret this as indicating, for instance, the existence of well defined icosahedra in krypton. Rather one should consider this information either comparatively or in terms of the general 'type' of ordering, e.g. close packed (fcc, hep) or open (diamond).

3.2 *Helium*

^{4}He undergoes a phase transition at the λ-point, $T_\lambda = 2.17$ K. Above this temperature it behaves as a normal fluid, while below it may be considered to be a mixture of normal fluid and superfluid with the superfluid concentration increasing as T decreases. It has generally been believed that the occurrence of the superfluid phase can be detected by a change in atomic structure. Pusztai and McGreevy[7] have used RMC to create three dimensional particle configurations of condensed ^{4}He that are consistent with diffraction data at ten different temperatures across the superfluid transition. They showed that all observable changes in the data are within the experimental uncertainties, so no conclusions can be drawn concerning possible structural differences between normal fluid and superfluid.

We will here consider just one of their results, that for helium-4 at 2.80 K and a density of 0.0226 Å^{-3}. The structure factor and RMC fit and the $g(r)$ and bond-angle distribution calculated from the RMC model are shown in Figure 4. The small shoulder on the left hand side of the first peak in $g(r)$ reflects the existence of systematic errors in the data being modelled. The structure factor is characteristically different

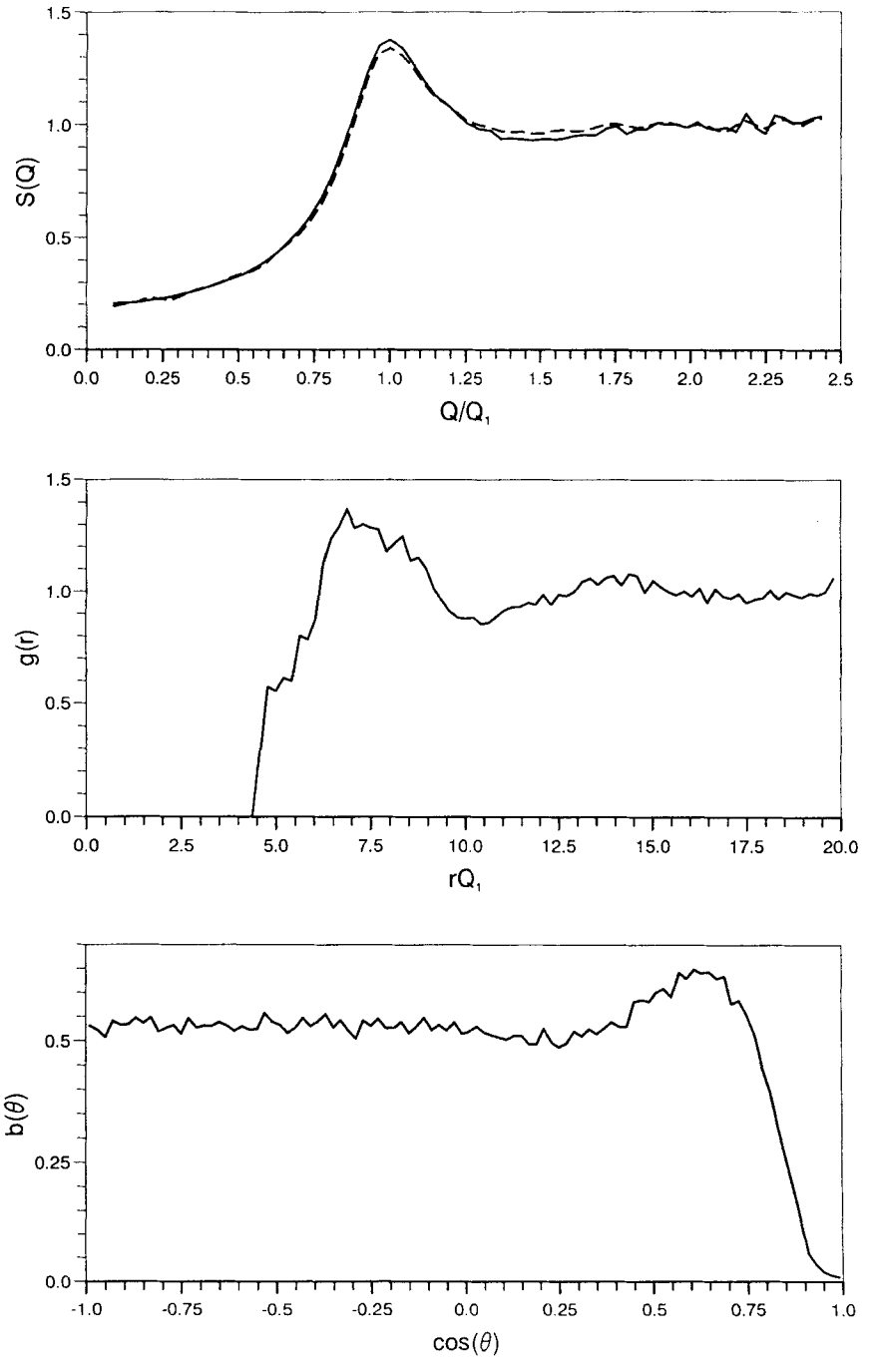

Figure 4 RMC results for liquid helium-4 at 2.8 K. Top: The experimental (solid line) and RMC (dashed line) $S(Q)$. Middle: $g(r)$. Bottom: $b(\theta)$.

from those of the simple liquids. The height of the first peak is significantly lower and there is a broad low Q tail. $g(r)$ has a correspondingly lower and broader first peak. The average coordination number is 11–12. The bond-angle distribution differs from those of the simple liquids, being virtually structureless for $\cos\theta \leq 0.25$ and peaking at $\cos\theta \approx 0.17$, slightly higher than for the simple liquids. The calculation of spherical harmonic invariants suggests that the local structure is dominantly icosahedral, as with other low density simple liquids.

3.3 *Weekly covalent liquids*

3.3.1 Group IIb: zinc and mercury The simple liquids are those in the periodic table from groups Ia to Ib, plus the rare earths (see Figure 1). As one moves into group IIb there is some evidence of increasing complexity. The first peak of the structure factor of zinc is slightly asymmetric, but not sufficiently so to enable any more detailed analysis without considerably more accurate data than are currently available; zinc has therefore been included with the simple liquids.

The structure factor and pair correlation function for liquid mercury look at first sight similar to those of the simple liquids. However, as we can see from Figure 5 where they are compared to the results for molten gold (chosen as a typical simple liquid), they are not quite the same. Here the scaling factor Q_1 has been chosen to make the high Q oscillations in $S(Q)$ coincide; this also makes the first peaks in $g(r)$ coincide. The first peak in the structure factor for Hg is now at a lower value of Q/Q_1, relative to that of Au, and can be seen to be slightly asymmetric. The first peak in $g(r)$ is correspondingly slightly more asymmetric on the high r side and the first minimum in $g(r)$ is higher. These are characteristic features which will be seen to develop further across the periodic table. As the first minimum in $g(r)$ becomes less well defined it is more difficult to decide how to define r_c. Consequently we have chosen, for all the liquids described in this section, to use the same relative value of $r_c Q_1$ as for Au, that is $r_c Q_1 = 10.6$. We shall indicate this average coordination number by $\langle n_{sl}\rangle$; for all the simple liquids $\langle n_{sl}\rangle \approx \langle n_c\rangle$. $\langle n_{sl}\rangle$ for Hg is then 12.4, in the simple liquid range. The bond-angle distribution is similar to those of the simple liquids and a spherical harmonic analysis suggests a similar local structure.

3.3.2 Group IIIb: aluminium, gallium, indium and thallium Aluminium and thallium have been categorised with the simple liquids. Results for gallium and indium are shown in Figure 6. We see that the asymmetry in the first peak of $S(Q)$ has now developed into a shoulder on the high Q side, this being stronger for Ga. The first peak is again at lower Q. $g(r)$ differs little except that the first peak is slightly higher, and possibly narrower, than is usual for the simple liquids. $\langle n_{sl}\rangle$ is 12.5 for both gallium and indium. The bond-angle distribution and spherical harmonic analyses again indicate that the local order is similar to that of the simple liquids.

3.3.3 Group IVb: silicon, germanium, tin and lead The experimental data available for molten silicon appears to contain significant systematic errors and we are not

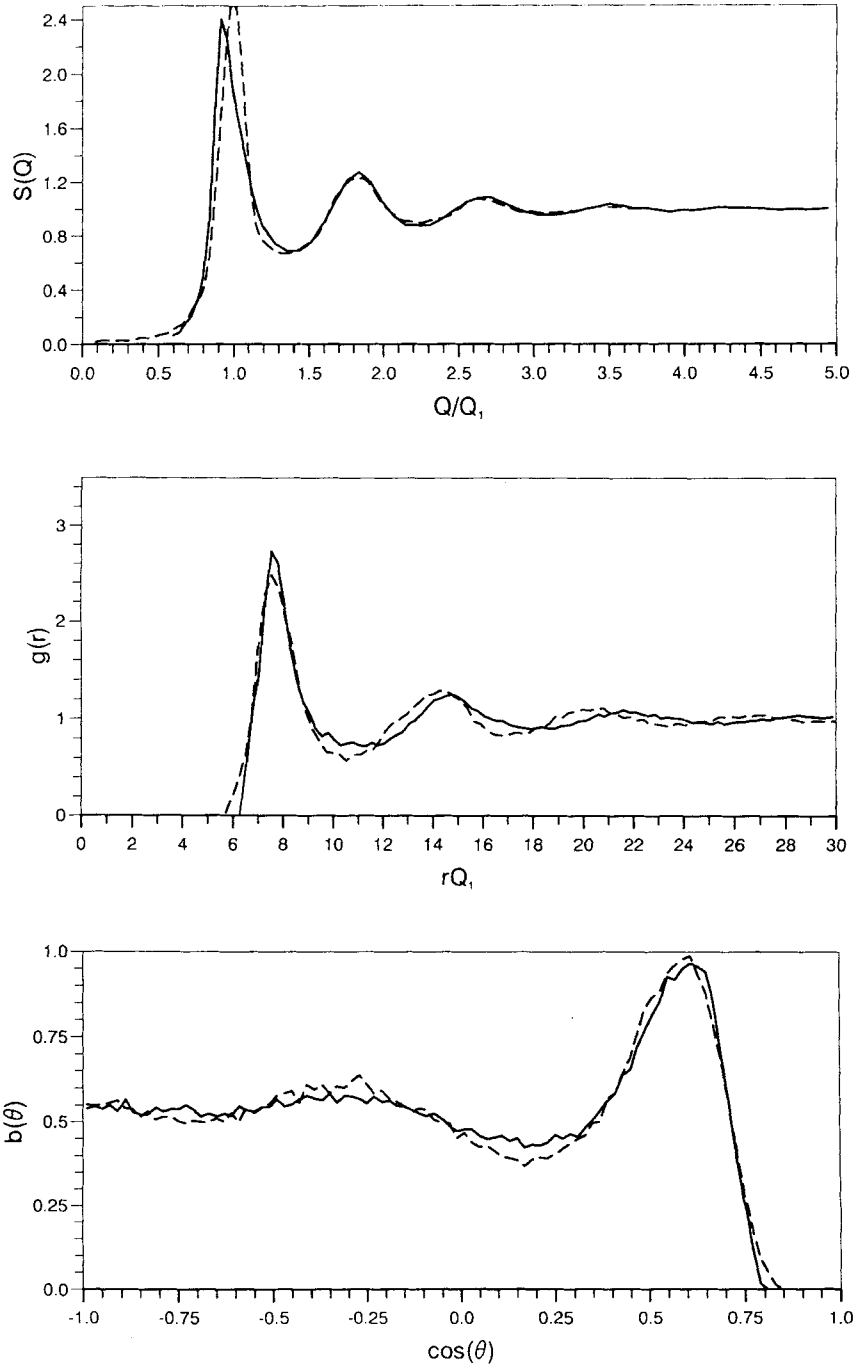

Figure 5 RMC results for liquid mercury (solid line) compared with those for gold (dashed line). Top: $S(Q)$. Middle: $g(r)$. Bottom: $b(\theta)$.

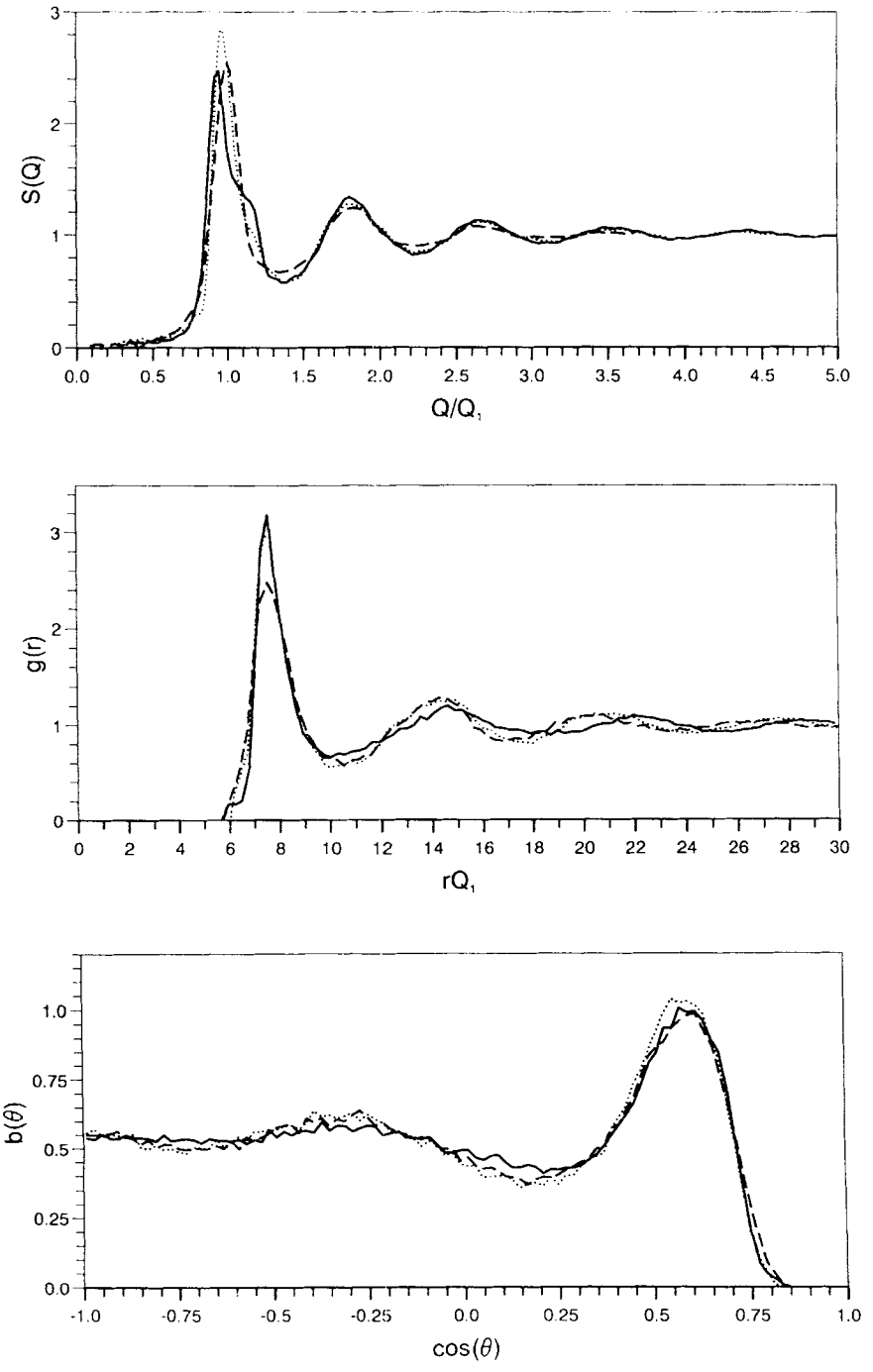

Figure 6 RMC results for molten gallium (solid line) and indium (dotted line) compared with those for gold (dashed line). Top: $S(Q)$. Middle: $g(r)$. Bottom: $b(\theta)$.

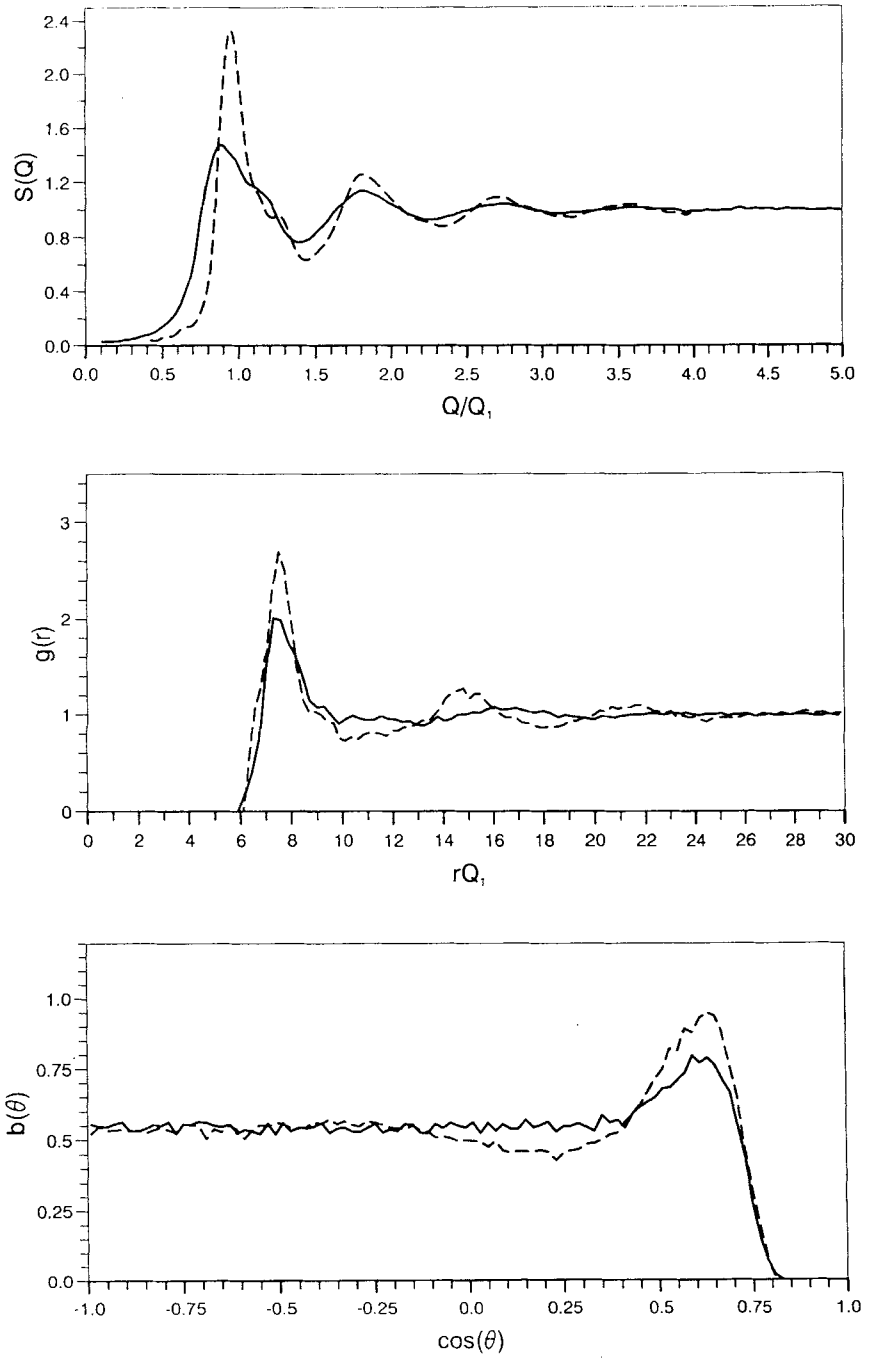

Figure 7 RMC results for molten germanium (solid line), and tin (dashed line). Top: $S(Q)$. Middle: $g(r)$. Bottom: $b(\theta)$.

able to obtain good fits. However the model we do derive shows all the same features as that for germanium described below.

Lead has been categorised with the simple liquids, but detailed work by others[9] has shown that the structure factor cannot be exactly described by a pairwise additive potential. We show the RMC results for tin in Figure 7. The structure factor is similar to that of Ga, i.e. the main peak occurs at $Q/Q_1 < 1.0$ and there is a shoulder on the right hand side. $g(r)$ now also has an observable shoulder on the right hand side of its first peak and the minimum is not well defined. $\langle n_{sl} \rangle$ is 12.6. $b(\theta)$ shows less structure than for the simple liquids; the peak at $\cos\theta \approx 0.5$ is lower, the minimum at ≈ 0.2 is higher and there is only a weak peak at ≈ -0.13, but the spherical harmonic analysis still suggests a dominantly close packed local structure.

We have obtained an excellent fit to both neutron and X-ray data for molten germanium. $S(Q)$ is significantly different (see Figure 7). The first peak is much lower and the shoulder much stronger. The peak in $g(r)$ is also low and asymmetric and the first minimum is very weak and ill defined so that it is impossible to define r_c and hence to determine $\langle n_c \rangle$. $\langle n_{sl} \rangle$ is 9.5, significantly lower than for the simple liquids. $b(\theta)$ only shows a single peak at $\cos\theta \approx 0.65$ and is otherwise flat. Spherical harmonic analyses suggests that the local structure is diamond-16, i.e. diamond structure with overlap of first (4) and second (12) coordination shells. Taking this together with the relatively low average coordination number and the ill defined first minimum it is possible to suggest that when germanium melts there is a partial collapse of the diamond structure towards a more close packed structure, but that there is still significant covalent bonding even though molten germanium is metallic.

3.3.4 Group Vb: bismuth and antimony The structure factors of bismuth and antimony are characterised by the presence of a distinct shoulder, indeed almost a peak, on the high Q side of the first peak in $S(Q)$ at a higher Q/Q_1 than for the elements we have already discussed. The first peak in $g(r)$ is somewhat similar and appears to be a combination of a tall narrow peak at $rQ_1 \approx 8$ and a lower broader one at $rQ_1 \approx 10$. The first minimum in $g(r)$ is then shifted to $rQ_1 \approx 12.6$, compared to 10.6 for the simple liquids. In a simple sense these features may be understood to indicate the presence of two equilibrium interatomic separations, though one is dominant. These two separations are due to competition between metallic and covalent bonding. The RMC results are shown in Figure 8.

$\langle n_{sl} \rangle$ is 11.5 for Bi and 12.6 for Sb, comparable to the simple liquids. $b(\cos\theta)$, apart from a peak at $\cos\theta \approx 0.65$, is relatively featureless. Spherical harmonic analysis gives diamond-16 and hcp as possible structures for Bi, and hcp, diamond-16 or bcc-14 for Sb. As with Ge this is indicative of a weak tendency towards a more open local structure, but close packing still dominates.

3.4 *Strongly covalent liquids*

It may be possible to represent the interactions in a liquid such as bismuth, where three body interactions are obviously required but weak, by an effective two body interaction. In this case RMC should produce a reasonable model of the structure

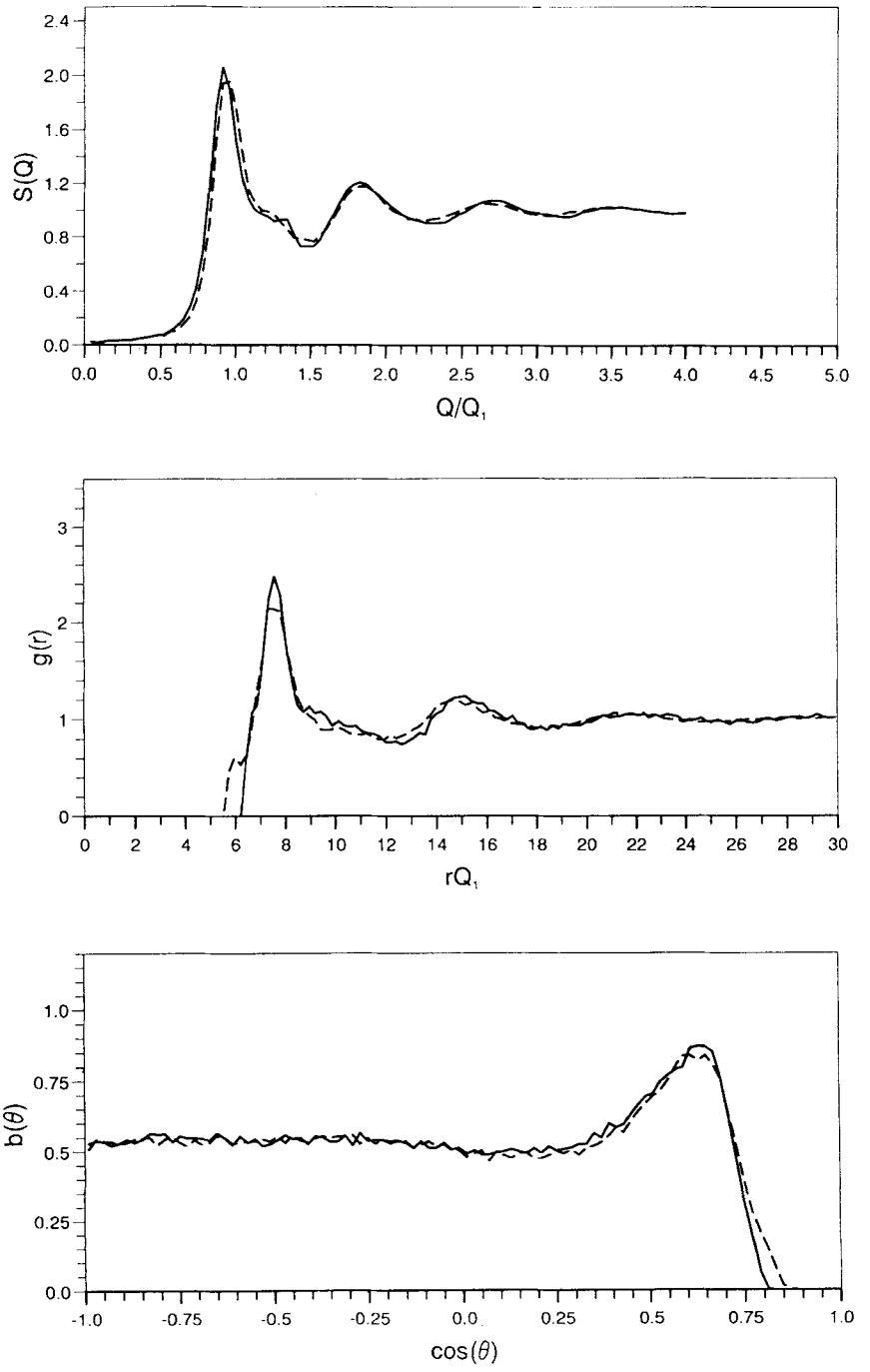

Figure 8 RMC results for molten bismuth (solid line), and antimony (dashed line). Top: $S(Q)$. Middle: $g(r)$. Bottom: $b(\theta)$.

without constraints. However more complex structures occur for elements such as arsenic, selenium, and tellurium where covalent bonding has greater importance. They are not, however, entirely molecular so three body terms are important but suitable constraints to use in RMC modelling are not obvious. For completely molecular liquids such as phosphorus, sulphur, nitrogen and the halogens, coordination constraints can be used to produce flexible molecules, or rigid molecules can be used directly.

3.4.1 Group Vb: arsenic, phosphorus and nitrogen The data for As have been recorrected on account of an apparently incorrect subtraction of the scattering from the silica sample container used in the experiment; this produced a strong negative peak in $g(r)$ at $\approx 1.6\ \text{Å}^{-1}$ corresponding to the Si–O bond length. Without this correction it was not possible to obtain a good fit to the data. The RMC fit is shown in Figure 9. The shoulder on the high Q side of the first structure factor peak for Bi and Sb has now grown into a distinct peak; correspondingly the shoulder in $g(r)$ has become the second peak and there is a distinct first minimum. The average coordination number up to this minimum is $\langle n_c \rangle = 3.75$, while $\langle n_{sl} \rangle = 6.1$.

$g(r)$ for amorphous arsenic has a sharp first peak and a minimum $g(r_c) \approx 0$, i.e. there is a well defined bond length and coordination number[10]. The value of 3.07 is consistent, with errors, with 3-fold coordination as in the crystal. Bellisent *et al.*[13] suggest that this is maintained on melting and quote a coordination number of 3.00 for the liquid. However the shapes of $g(r)$ and $S(Q)$ for liquid As differ significantly from those of amorphous As. The fact that our coordination number is larger than that of Bellisent *et al.* is partly because we have recorrected their data. However even when we use their original data we find a coordination number of 3.64. We therefore suggest that, while 3-fold coordination may dominate, other coordinations occur. This is consistent with the fact that $g(r_c) \approx 0.8$, i.e. the first minimum is not close to zero so there is overlap of first and second coordination shells. In fact the coordination number distribution peaks between 3 and 4 but ranges from 0 to 8.

The bond angle distribution (Figure 9) is now significantly different from the simple liquids. There are strong peaks at 60°, 90° and 180°. Because the covalent bonding is strong it will not now be possible to describe liquid arsenic using a pairwise additive potential, so RMC will not correctly reproduce the three body correlations. However, since the liquid is also not entirely molecular and does not have a well defined coordination, there are no suitable constraints that can be used. It is not logical to attempt to maximise the 3-fold coordination since $\langle n_c \rangle$ is significantly larger than 3.

Liquid phosphorus is well known to be molecular. The experimentally determined $g(r)$ has a sharp first peak and then decreases to zero with $\langle n_c \rangle \approx \langle n_{sl} \rangle \approx 3$. This is consistent with the existence of P_4 molecules, which are known to be stable in the vapour phase. The structure factor (Figure 10) is quite different from that of As (Figure 9). The sharp first peak at $Q/Q_1 = 0.42$ and the small second peak at 0.73 are essentially the structure factor for the inter-molecular correlations and the subsequent peaks are the molecular form factor, i.e. intra-molecular correlations.

We have modelled phosphorus in three different ways. Firstly we have used RMC with no constraints; for such strongly covalent bonding this would not be expected

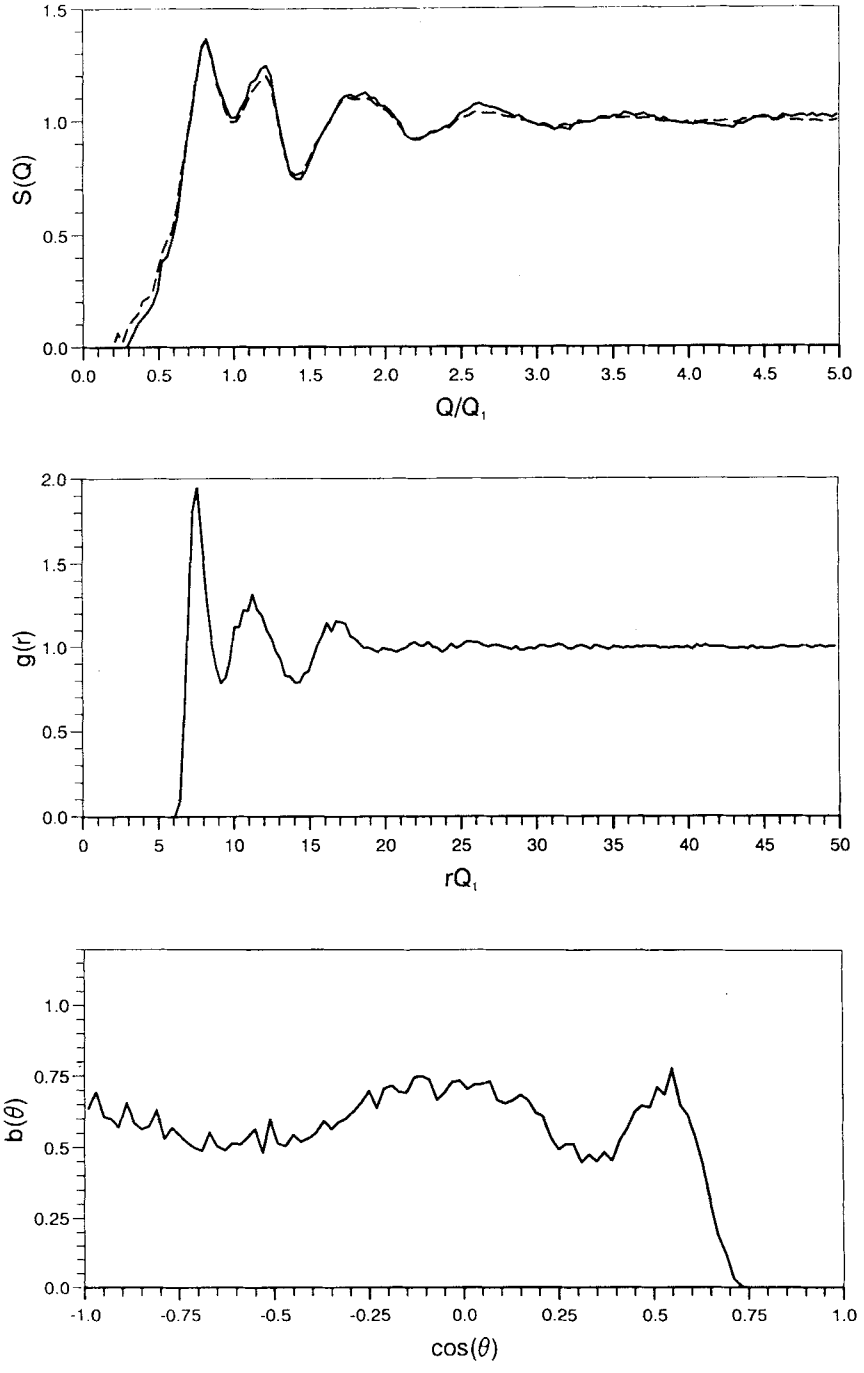

Figure 9 RMC results for liquid arsenic. Top: The experimental (solid line) and RMC (dashed line) $S(Q)$. Middle: $g(r)$. Bottom: $b(\theta)$.

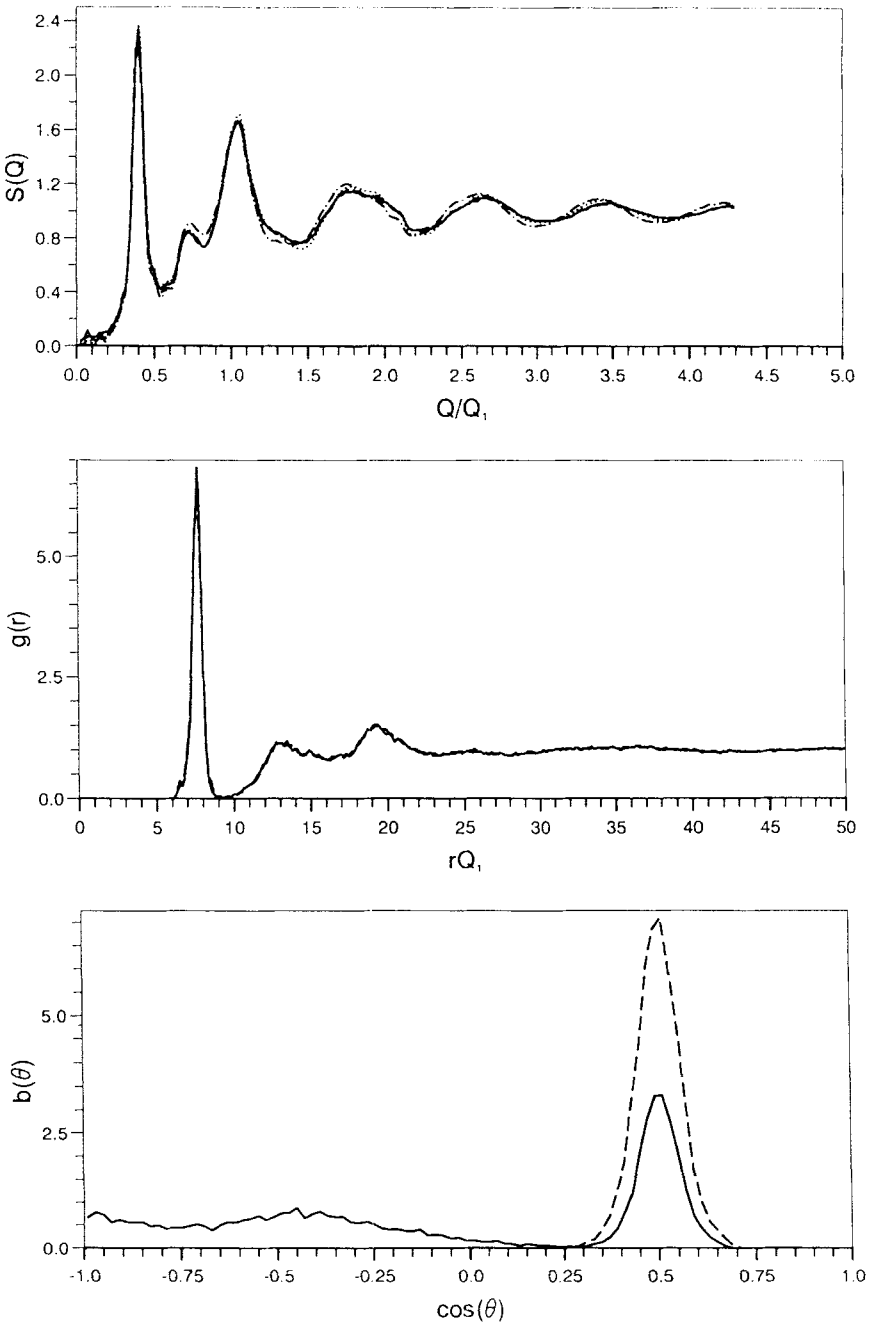

Figure 10 RMC results for phosphorus. Top: $S(Q)$ showing experimental data (dotted line) and RMC results for unconstrained fit (solid line), for P_4 coordination constrained model (dashed line) and for P_4 rigid molecule model (dash-dot line). Middle: $g(r)$ for unconstrained fit (solid line) and for P_4 coordination constrained model (dashed line). Bottom: $b(\theta)$ for unconstrained fit (solid line) and P_4 coordination constrained model (dashed line).

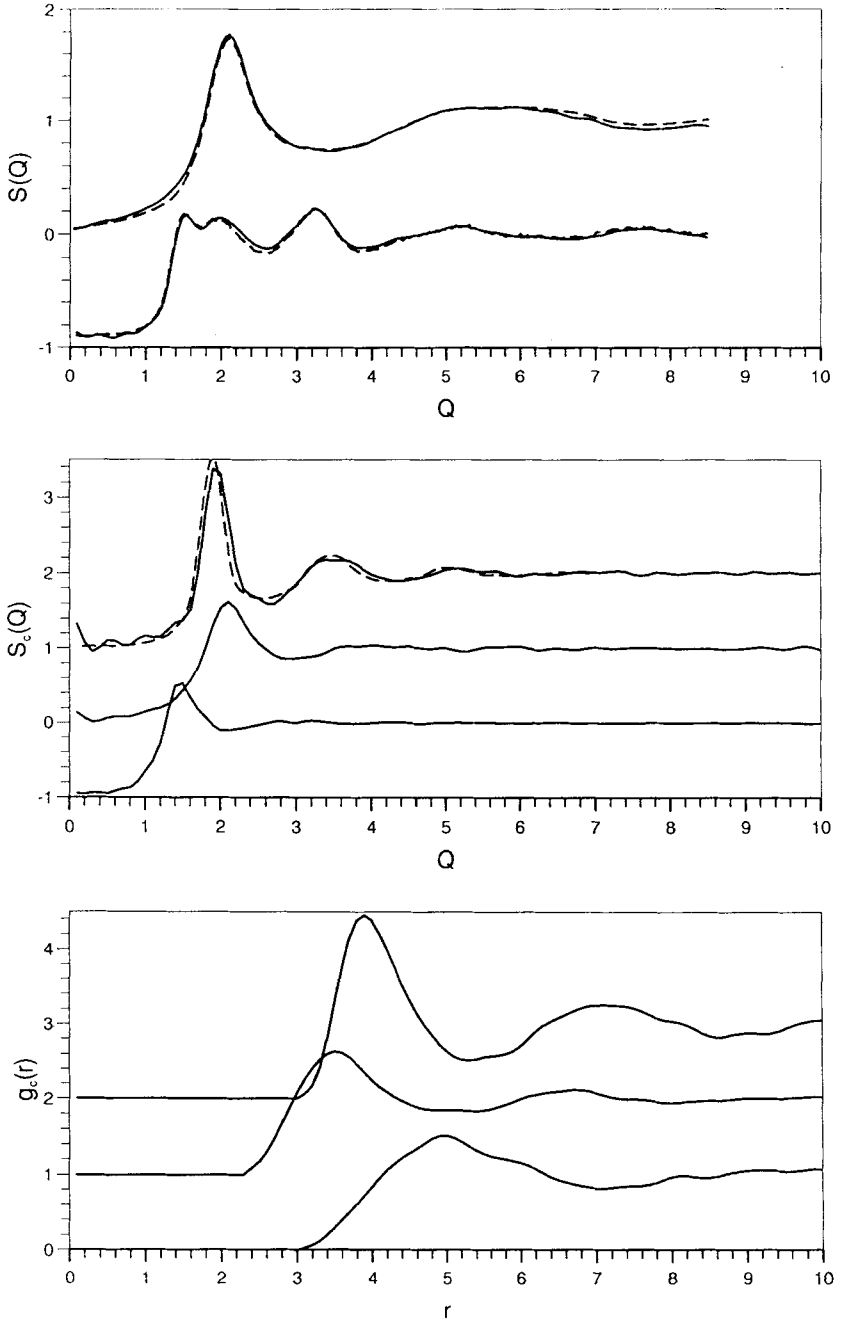

Figure 11 RMC results for diatomic molecules. Top: $S(Q)$ showing experimental data (solid line) and RMC fit (dashed line) for fluorine (upper curves) and iodine (lower curves). Middle: $S_c(Q)$ for, from a top to bottom, nitrogen, fluorine, and iodine. $S_c(Q)$ for nitrogen is compared to a $S(Q)$ for a simple liquid (dashed line). Bottom: $g_c(r)$ for, from top to bottom, nitrogen, fluorine, and iodine.

to reproduce the correct three body correlations. Secondly we have used a constraint of 3-fold coordination, starting from a configuration of P_4 molecules; this produces flexible molecules. Thirdly we have used rigid P_4 molecules. The rigid molecule model does not fit the data as well as the other two, indicating that some molecular distortion is required. This is consistent with the width of the first peak in the experimental $g(r)$ which is greater than expected from the Q range of the data. The experimental $S(Q)$ and RMC fits are shown in Figure 10. For the unconstrained fit the bond angle distribution has a peak at 60° and secondary peaks at higher angles. The flexible molecule model has only the 60° peak with a width of $\pm 15°$. For the rigid molecule $b(\cos\theta)$ is of course a delta function at 60°. The angular correlations in phosphorus will be discussed in detail in a separate paper.

Liquid nitrogen consists of diatomic molecules and the data can be fitted well using rigid molecules[5]. The structure factor for molecular centres, $S_c(Q)$, and the corresponding radial distribution function, $g_c(r)$, are shown in Figure 11. It can be seen that $g_c(r)$ is very similar to a simple liquid $g(r)$ indicating simple pairwise additive inter-molecular forces.

3.4.2 Group VIb: tellurium, selenium and sulphur The structure factor for tellurium is shown in Figure 12; it is quite similar to that for arsenic (Figure 9), as is $g(r)$. There is a well defined first minimum in $g(r)$ but the height is 0.9 so there is considerable overlap of first and second coordination shells. $\langle n_c \rangle \approx 2.6$ while $\langle n_{sl} \rangle \approx 5.5$. The latter value is far lower than that for simple liquids but much larger than the former. Clearly the liquid is not molecular; there is strong covalent bonding but still some influence of close packing. It is often considered that chain formation, i.e. 2-fold coordination, is an important feature of the structures of elements in this group. However since the minimum is $g(r)$ is not low and $\langle n_c \rangle$ is larger than 2 there is no sensible way of using coordination constraints.

$S(Q)$ for selenium (Figure 13) is significantly different from that for tellurium, with the first peak being very broad and low. It can be seen to be intermediate between that for tellurium (Figure 12) and sulphur (Figure 14). $g(r)$ has a well defined first minimum but $\langle n_c \rangle = 2.9$, rather than 2 as would be expected for a chain structure. This might possibly be due to errors in the data, though there is no particular evidence to support such an idea. A good fit to the data can in fact be obtained with high degree of 3-fold coordination, though from a knowledge of the crystal structure and chemistry of selenium this would not be a logical choice. $b(\cos\theta)$ is similar to those for arsenic and tellurium, but the central peak occurs at 105°, rather than 95°, indicating a slightly larger bond angle and more open structure.

An excellent fit has been obtained to $S(Q)$ for sulphur (Figure 14). $g(r)$ has a sharp first peak and low first minimum, with $\langle n_c \rangle \approx \langle n_{sl} \rangle \approx 2$. This indicates a highly molecular liquid. We have modelled sulphur in three different ways – using no constraints, maximising 2-fold coordination (to about 96%) to produce a 'chain' model, and with flexible S_8 ring molecules. Details will be discussed in a separate paper. However it is worth noting here that the fits to the data are almost identical; this is not surprising since the difference between an S_8 ring and chain involves an 8-body correlation function, whereas $S(Q)$ is only a 2-body correlation function.

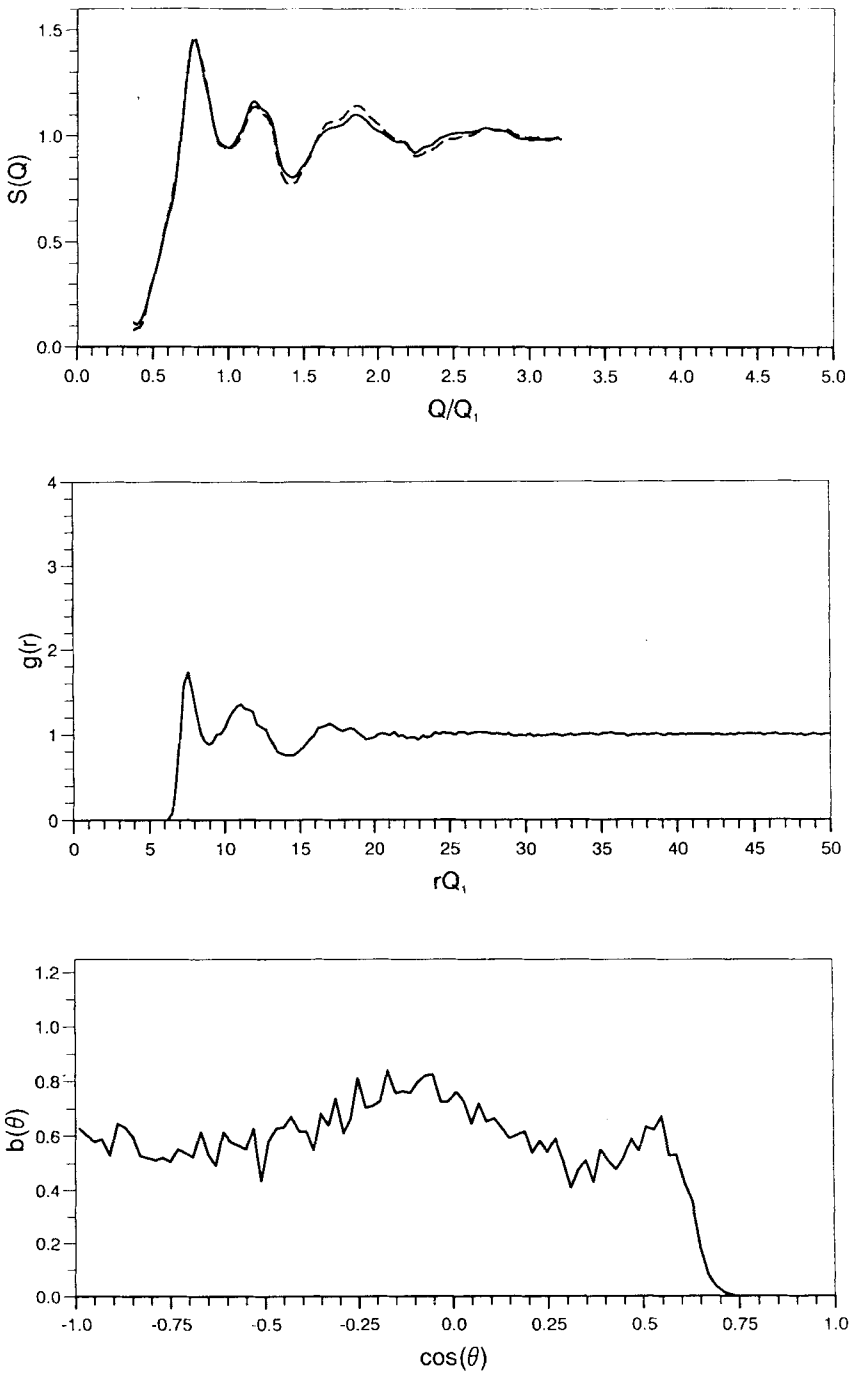

Figure 12 RMC results for molten tellurium. Top: The experimental (solid line) and RMC (dashed line) $S(Q)$. Middle: $g(r)$. Bottom: $b(\theta)$.

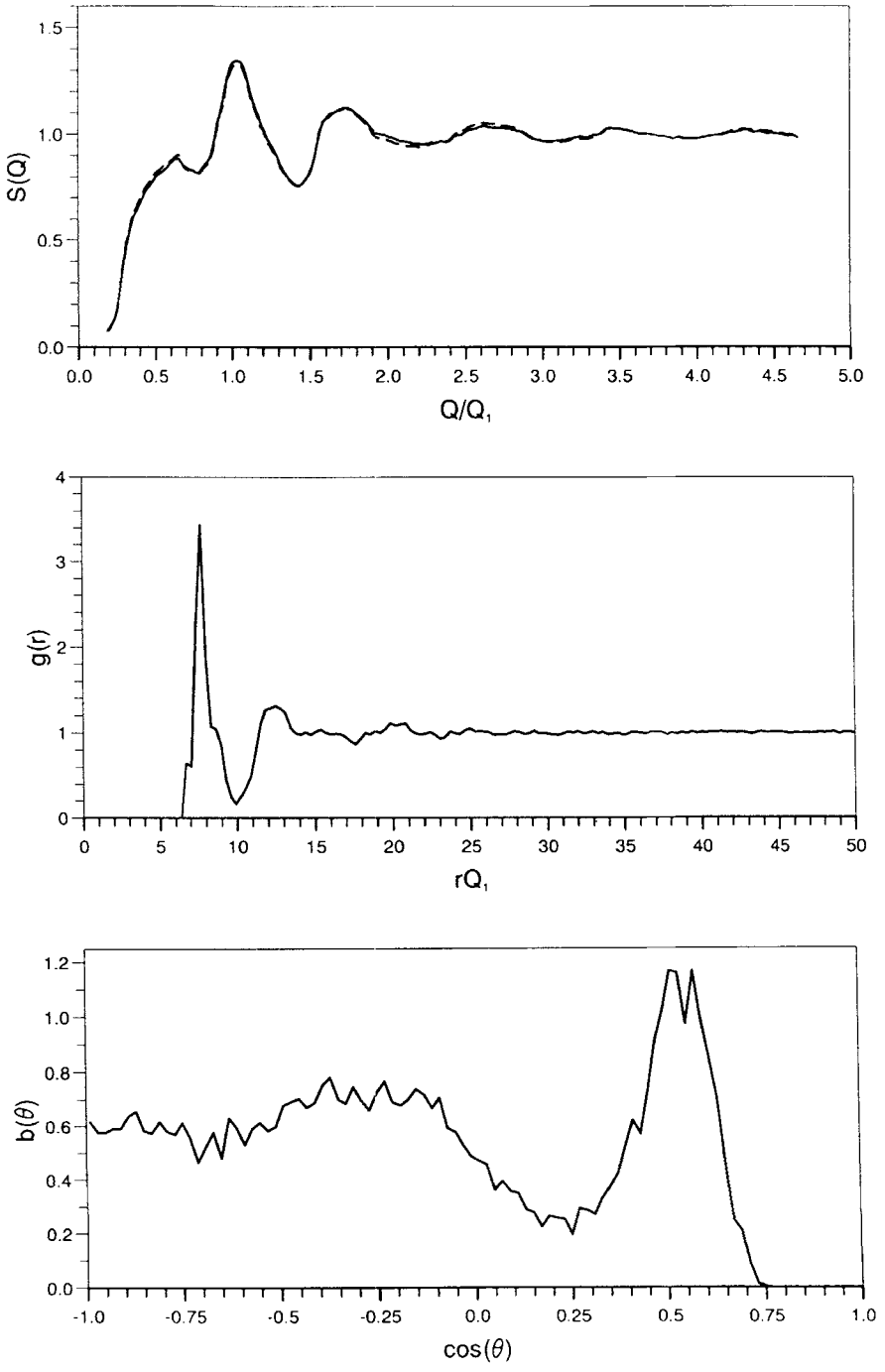

Figure 13 RMC results for molten selenium. Top: The experimental (solid line) and RMC (dashed line) $S(Q)$. Middle: $g(r)$. Bottom: $b(\theta)$.

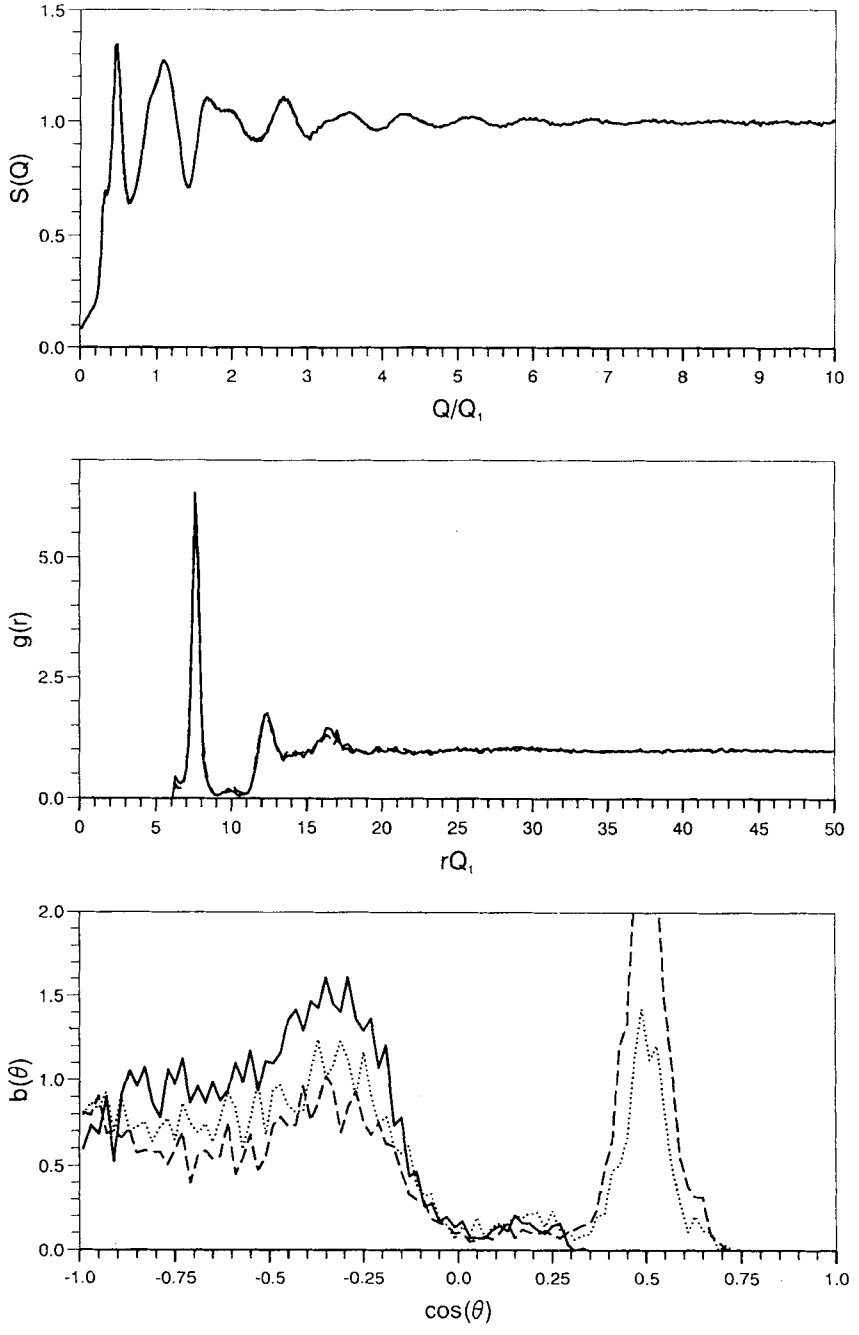

Figure 14 RMC results for molten sulphur. Top: $S(Q)$ at 130°C showing experimental data (solid line) and RMC results for unconstrained fit (dashed line) and ring model (dotted line). Middle: $g(r)$ at 130°C (solid line) and 220°C (dashed line). Bottom: $b(\theta)$ for molten sulphur at 130°C obtained from ring model (solid line), chain model (dotted line) and unconstrained fit (dashed line).

$b(\cos\theta)$ is shown in Figure 14. For the unconstrained model there is a sharp peak at 60° due to the existence of a small number of equilateral triangles (the peak is large because the triangles are necessarily well defined). These probably do not exist in reality and their number is decreased in the chain model. It would be possible to include a constraint to remove them but this would be computationally expensive and was not felt to be worthwhile at present.

3.4.3 Group VIIb: the halogens The structures of the diatomic molecular liquid halogens have already been discussed in detail by Howe[5]. Examples of RMC fits are shown in Figure 11, together with the molecular centres correlation functions from the RMC models. They are similar for all four halogens with the structure factors $S_c(Q)$ being relatively featureless apart from a single peak corresponding to the rapidly decaying oscillations in $g_c(r)$. Liquid nitrogen differs by having oscillations in $g_c(r)$ extending over a much longer distance indicating longer range positional correlations. $g_c(r)$ for the halogens is different from a simple liquid $g(r)$, indicating more complex intermolecular interactions than for nitrogen.

One way of considering orientational correlations in diatomic molecular liquids is in terms of a spherical harmonic expansion[11,12] of the molecular pair correlation function $g(r, \theta_1, \theta_2, \phi)$. This function is the equivalent of $g(r)$ for atoms but depends not only on the distance, r, between the molecular centres but on the relative orientations of the molecules. It is possible to expand this function as an infinite series of the orthonormal set of spherical harmonics. A study of these functions calculated from the RMC results[5] has lead to the conclusion that orientational correlations are largely confined to the nearest neighbour coordination shell. They can partly be accounted for by geometric factors although there is an increased tendency in the halogens for neighbouring molecules to be aligned end to end which contrasts with what would be expected from a purely quadrupole interaction. The differences between the structure factors of the different halogens are a result of the different elongations and anisotropic interactions of the molecules.

3.5 *Electron correlations*

There are a number of studies in the literature where the differences between the structure factors measured by X-ray and neutron scattering have been used to derive information about electron correlations, since the X-ray structure factor is determined by the electron density distribution and the neutron structure factor by the nuclear density distribution. We have fitted both X-ray and neutron data for molten lithium and germanium; these both have a relatively high ratio of bonding to core electrons and so any effects might be expected to be relatively large. The available data is also of good quality. We have found that the (small) differences between the X-ray and neutron data are within the errors and hence no conclusions can be drawn about electron correlations. Given the experience we have gained throughout this work of the general level of systematic errors in liquid structure factors we would suggest that suitably accurate data for determination of electron correlations are not yet available.

4 DISCUSSION

4.1 *Three body correlations*

It has been stressed earlier that, for liquids where 3-body forces are significant (strong covalency), one would not expect RMC to produce exactly the 'right' structure. However it is clear that it nevertheless produces an indication of the structural trends, and the following discussion should be taken as referring to those trends, rather than making absolute statements about the structure of particular liquids.

The trends in 2-body correlations with increasing covalency are seen most clearly in terms of $\langle n_{sl} \rangle$. While we have previously criticised the use of average coordination numbers as a significant way of categorising a structure[4] this criticism was based on the use of $\langle n_c \rangle$ as an absolute number, particularly when the first minimum in $g(r)$ is poorly defined. Here we will use the average coordination number $\langle n_{sl} \rangle$ as defined earlier; the radius for calculation of the coordination number has then been defined in the same relative way for all the liquids and the coordination number itself is only used as a relative quantity. For the simple liquids and most of the weakly covalent liquids (as categorised above) $\langle n_{sl} \rangle \approx 13$ (see Figure 1 and Table 3), i.e. one can consider that if $\langle n_{sl} \rangle / 13 \approx 1$ then close packing dominates the structure. The first significant deviation from this on moving across the periodic table occurs for germanium in group IVb, where $\langle n_{sl} \rangle / 13 \approx 0.75$. Close packing still dominates but there are significant effects of covalency. For arsenic and tellurium $\langle n_{sl} \rangle / 13 \approx 0.5$ so these may be considered intermediate, while for selenium $\langle n_{sl} \rangle / 13 \approx 0.5$ but $\langle n_{sl} \rangle$ is greater than $\langle n_c \rangle$ so the system is not entirely molecular.

Table 3 Some parameters for the weakly and strongly covalent liquids

Element	*Temperature* °C	*Density* ($Å^{-3}$)	Q_1 ($Å^{-1}$)	$\langle n_c \rangle$	$\langle n_{sl} \rangle$
As	825	0.0419	3.05	3.75	6.1
Bi	293	0.0289	2.30	—	11.5
Br	20	0.02352	—	1.0	—
Cl	22	0.02384	—	1.0	—
F	−196	0.0495	—	1.0	—
Ga	20	0.5272	2.71	—	12.5
Ge	1000	0.0456	2.81	—	9.5
Hg	20	0.04068	2.51	—	12.4
I	120	0.0185	—	1.0	—
In	166	0.0368	2.40	—	12.5
N	−208	0.03702	—	1.0	—
P	50	0.03455	3.5	2.9	3.1
S	130	0.0335	3.7	1.92	2.2
Sb	658	0.0322	2.3	—	12.6
Se	265	0.0248	3.2	2.9	3.1
Sn	250	0.0345	2.35	—	12.6
Te	450	0.0272	2.7	2.6	5.5

The structural changes with increasing covalency can be seen more clearly in terms of the 3-body correlation function $g(r, \cos\theta)$. We define the y axis by the vector joining an atom and its nearest neighbour. The distribution of all other atoms is then calculated as a function of their distance from the central atom, $r = |\mathbf{r}|$, and the angle θ between $\mathbf{r}$ and the y axis. This is averaged over all atoms as centres. Note that $\int_0^{r_c} g(r, \cos\theta) \neq b(\cos\theta)$, since the angular distribution is taken relative to the nearest neighbour only, not relative to all neighbours within r_c.

An example of $g(r, \cos\theta)$ for a simple liquid (lead) is shown in Figure 15. The distribution of nearest neighbours occurs along the line $\cos\theta = 1$ (since they define this axis) at $r \approx 3$ Å. The first coordination shell is the ridge along $r \approx 3.3$ Å and the second coordination shell the very weak ridge along $r \approx 6.2$ Å. The first shell has a strong maximum at $\cos\theta \approx 0.45$ ($\theta \approx 60°$), a weaker maximum at -0.45 (120°) and a weak maximum at -1.0 (180°). (Some features of $g(r, \cos\theta)$ described are, unfortunately, not particularly clear in a black and white contour plot, but are obvious in colour.) The comparable maxima in $b(\cos\theta)$ occur at $\cos\theta = 0.6$, -0.3 and -1

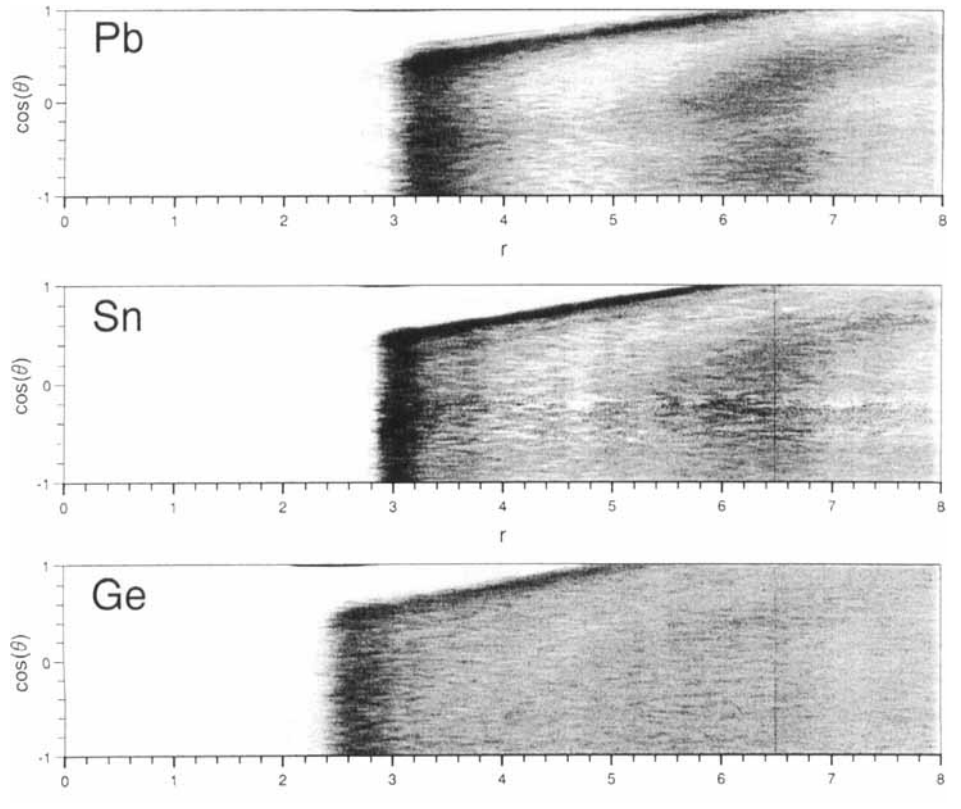

Figure 15 Contour plots of $g(r, \cos\theta)$ for group IVb elements; lead, tin and germanium. Darker regions have higher density.

(see Figure 3). It might initially be thought that the 60° peak is simply indicative of 'hard sphere' triplets at the closest approach distance, but for a hard sphere liquid at an equivalent packing fraction this peak is actually much weaker. It is in fact indicative of a sharp peak in $g(r)$, i.e. if the distribution of neighbour distances in the first coordination shell is narrow and the coordination number is large there will be a large number of triplets with very similar interatomic separations and so a preponderance of bond angles around 60°. Because the nearest neighbour is used to define the axis the peak will occur at an angle slightly above 60°, i.e. $\cos\theta < 0.5$.

4.1.1 Group IVb: germanium, tin and lead $g(r, \cos\theta)$ for Pb has been described above. For Sn (Figure 15) the 60° peak in the first coordination shell is weaker and the 120° peak has spread from 120° to 95°. For Ge the 60° peak is very weak and the second peak is now centred around 104°, close to the tetrahedral angle of 109°. Note that $g(r, \cos\theta)$ shows more distinct angular correlations than $b(\cos\theta)$ (Figure 7). These results indicate a gradual change from a structure based on hexagonal close packing to one based on the diamond structure as the strength of covalent bonding increases from Pb to Sn to Ge. Clearly the preferred coordination number for covalent bonding would be 4.

4.1.2 Group Vb: bismuth, antimony, arsenic, phosphorus and nitrogen In Figure 16 we show $g(r, \cos\theta)$ for the group Vb elements. For phosphorus we have used a flexible P_4 molecule model, and for nitrogen a rigid N_2 molecule model.

$g(r, \cos\theta)$ for Bi is significantly different from that for the simple liquids (see e.g. Pb in Figure 15). The 60° peak in the first coordination shell is weak. The secondary peak occurs from 70°–100° and there is a minimum around 120°–130°, whereas the opposite is true for Pb. Also the 60° peak has a very slight 'spike' towards shorter distances. These results are indicative of a structure which is basically close packed, as for the simple liquids, with a very slight tendency to form tetrahedra (Bi_4) with a shorter bond length. Such tetrahedral units occur in the crystal structure. For Sb the results are less clear. The 60° peak is weaker and $g(r, \cos\theta)$ is still higher around 70°–100° and lower around 110°–130°. The lack of well defined features is quite similar to the case for germanium, so it is likely that this is caused by the structure being intermediate between close packing and covalency. For As the 60° peak is very weak and there is now a peak at 100°. Even though the angular correlations in the first coordination shell are weaker than for Bi or Sb there is weak evidence of particular angular correlations in the second and third shells. For phosphorus the first coordination shell is clearly seen at 60°, since the P_4 molecule is tetrahedral. There is a single strong peak at $\cos\theta \approx -0.75$ in the second coordination shell and a very weak one at 0.25. Three peaks can be seen in the third coordination shell, the strongest being at $\cos\theta \approx 0.8$, and a very weak peak in the fourth shell at a similar angle. These peaks are indicative of definite angular correlations between molecules; such correlations must occur since the P_4 molecules are strongly aspherical and yet closely packed. The intra-molecular correlations will be discussed in detail elsewhere. For nitrogen the second correlation shell in $g(r, \cos\theta)$ shows no strong features. This

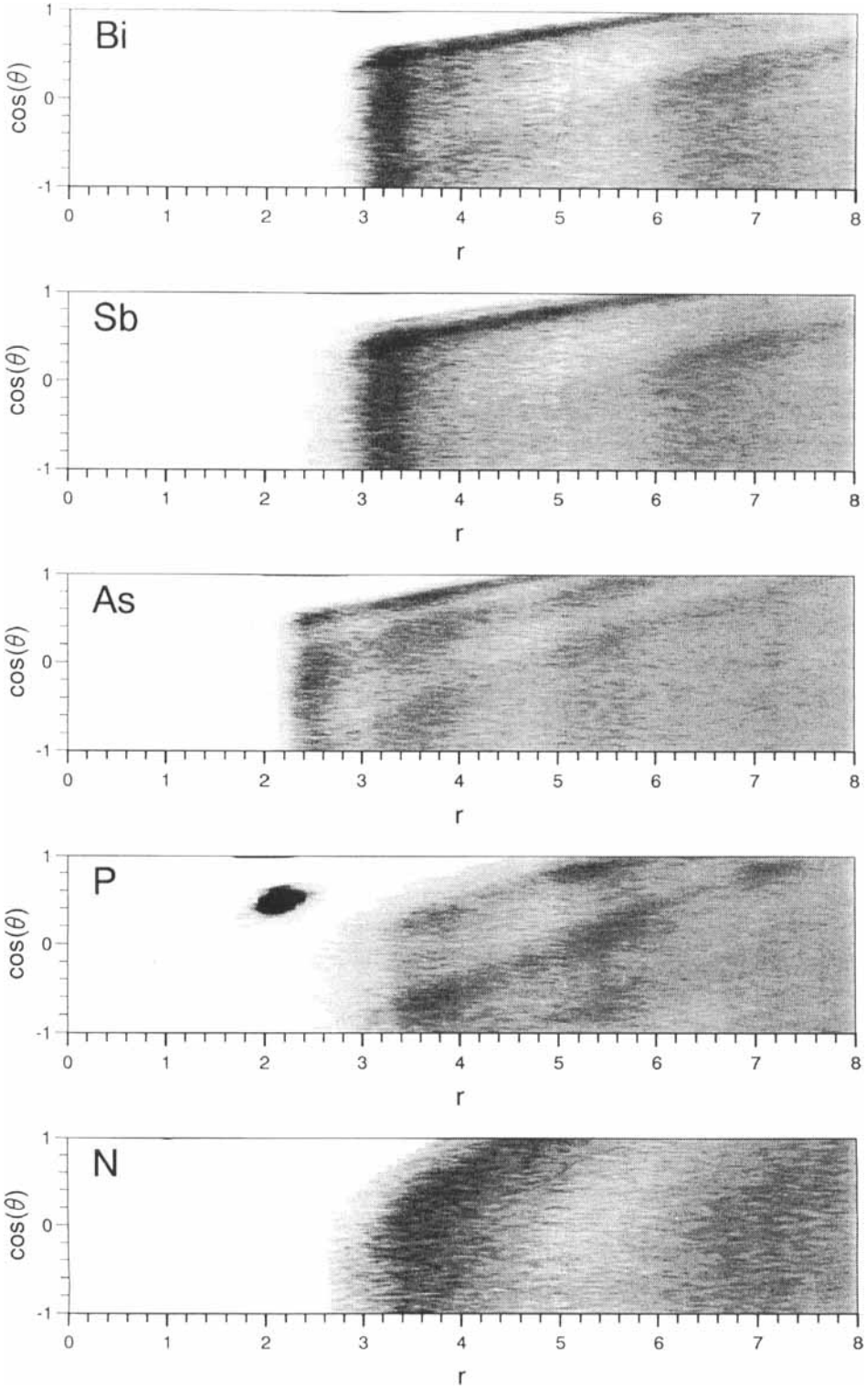

Figure 16 Contour plots of $g(r, \cos\theta)$ for group Vb elements, bismuth, antimony, arsenic, phorphorus and nitrogen. Darker regions have higher density.

is consistent with the simple liquid form of $g_c(r)$ (Figure 11), indicating no significant angular correlations between molecules.

The effect of an increasing tendency to covalency, which in the group Vb liquids means a tendency to 3-fold coordination, can be shown by a very simple model. We have run a conventional hard sphere Monte Carlo simulation with a fixed packing fraction, but have applied a coordination constraint in the manner described in section 2. The proportion of atoms, f_{req} (see Eq. 4), with 3-fold coordination between 3.65 Å (hard sphere diameter) and 4 Å has gradually been increased. The resulting structure factors are shown in Figure 17. As f_{req} increases the first peak in $S(Q)$ splits and then the higher Q side becomes dominant. At the same time oscillations at large Q become more pronounced. While this behaviour is clearly not identical to that observed in e.g. bismuth it does show how a shoulder/split first peak in $S(Q)$ can arise from a very weak local tendency to lower coordination (covalent bonding).

The trends within this group show that there is an increasing tendency to tetrahedral bonding from Bi → Sb → As → P. In the case of bismuth this is very weak,

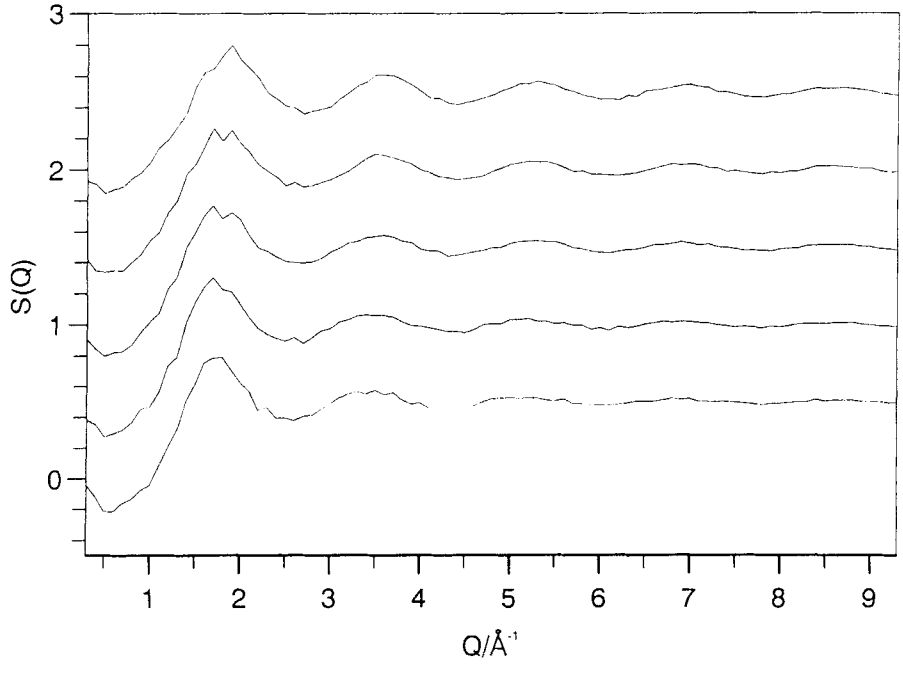

Figure 17 $S(Q)$ for hard sphere simulations with increasing 3-fold coordination between 3.65 and 4.0 Å (see text for details). The curves, successively offset by 0.5, are for 1.3%, 9.2%, 18.5%, 27.5% and 37.4% 3-fold coordination in ascending order.

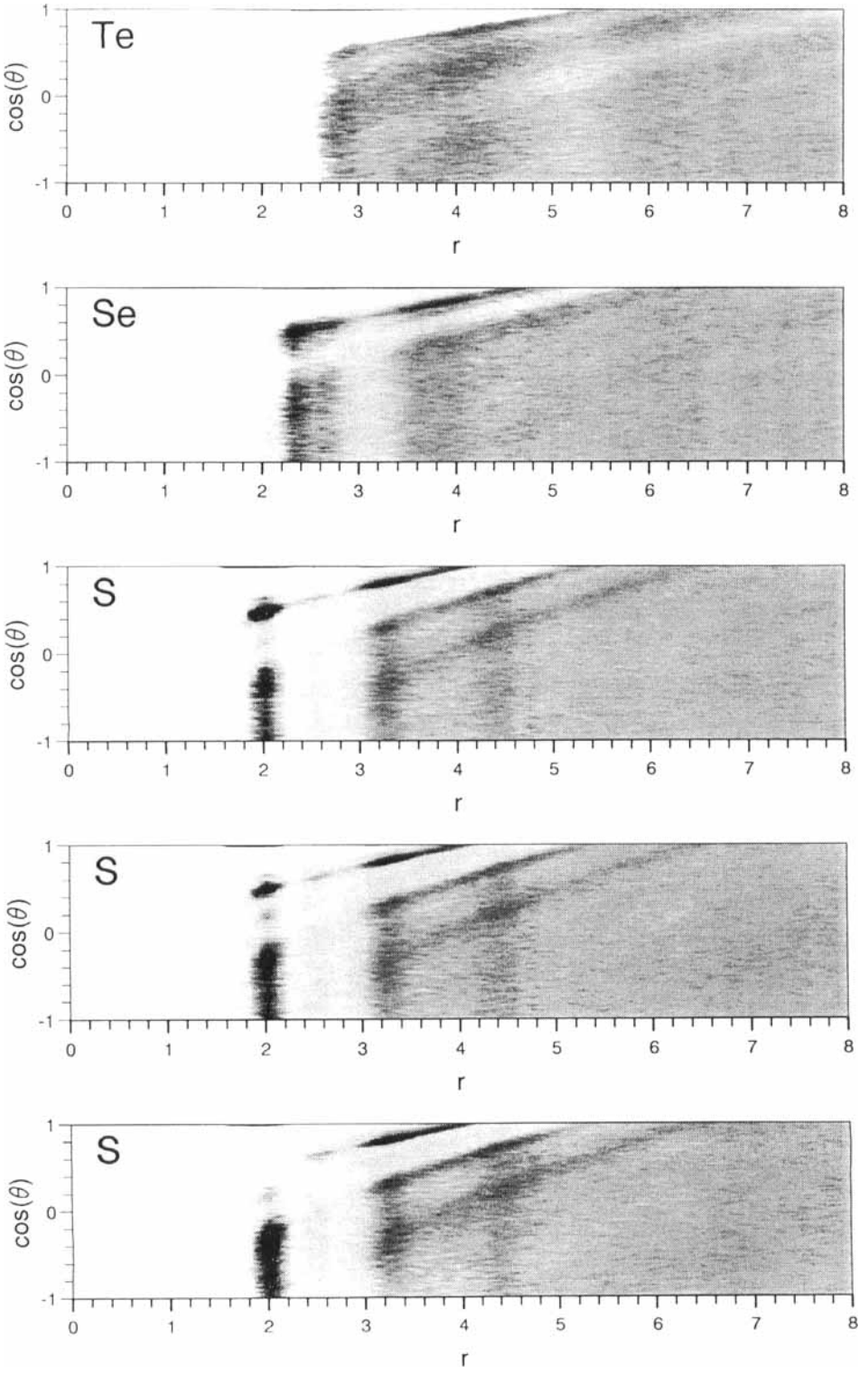

Figure 18 Contour plots of $g(r, \cos\theta)$ for group VIb elements; tellurium, selenium and sulphur. The three plots for sulphur refer to, in descending order, the unconstrained model, chain model and ring model. Darker regions have higher density.

yet sufficient to noticeably distort $S(Q)$ from that expected for close packing. In antimony it is stronger; this is more noticeable from $g(r, \cos\theta)$ than from $b(\cos\theta)$. For arsenic there is now a definite shift away from close packing to covalent bonding, but this is not sufficiently strong that permanent molecules are formed. Instead one could consider the structure as consisting of a mixture of quasi-molecular and close packed regions, but with rapid exchange of atoms between the regions.

4.1.3 Group VIb: tellurium, selenium and sulphur $g(r, \cos\theta)$ for tellurium, selenium and sulphur are shown in Figure 17. For sulphur we compare unconstrained, chain and ring models. In this group the expected preferential bonding is 2-fold coordination. In the case of tellurium $g(r, \cos\theta)$ is almost featureless; in fact second shell features are stronger than those in the first shell. Selenium has a well defined 60° peak in the first shell but this may be an artefact due to the existence of equilateral triangles as discussed above for sulphur. The unconstrained sulphur model has a similar peak, it is weaker for the chain model and absent for the ring model. However,

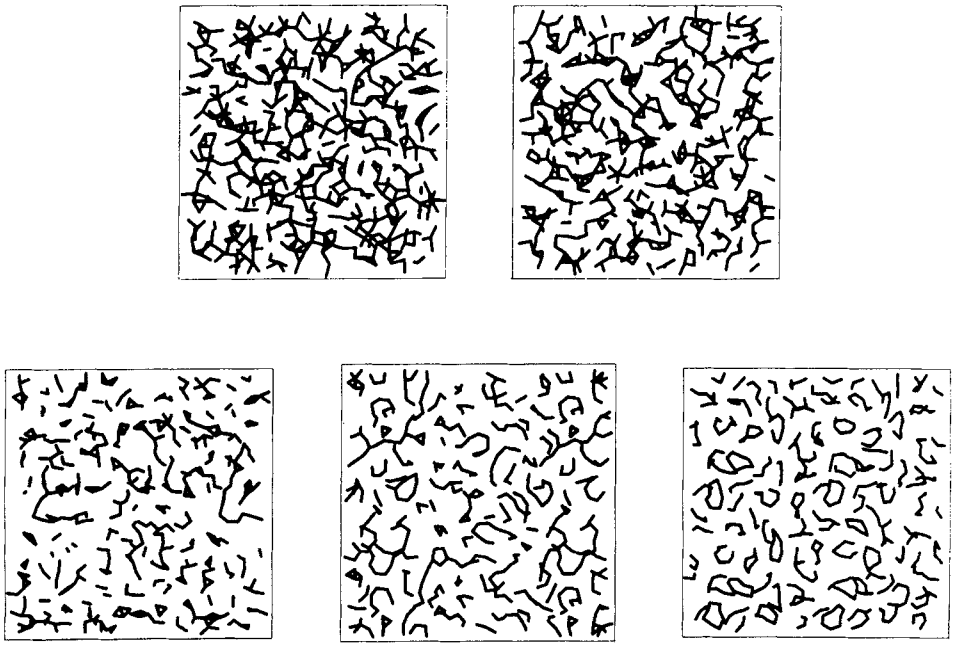

Figure 19 5 Å thick sections of RMC models of tellurium (top left), selenium (top centre) and sulphur (unconstrained model—top right, chain model—bottom left, ring model—bottom right).

the other features are similar. We would therefore suggest that the 60° peak be ignored for selenium and sulphur. One can then see that there are clear trends in going from Te → Se → S; features occur in similar relative positions and simply strengthen with increasing covalency. The trends can also be shown by direct examination of the RMC models. In Figure 19 we show 10 Å sections of configurations; bonds are drawn between atoms and their neighbours, these being defined as those closer than r_c. The structures consist of cross-linked and broken chains. The degree of cross linking decreases from Te → Se → S, the chains thus becoming more obvious. In the case of the unconstrained model for sulphur there are a significant number of unbonded atoms. However recall that this model is not supposed to represent the real structure, merely to reflect the trends within the group. A section of the chain model is also shown in Figure 19. The number of unbonded atoms is now small and the chain length is clearly greater. We can thus conclude that the basic idea of chain structures within this group is probably correct, but for tellurium and to a lesser extent selenium the chains are cross-linked and broken. The ring model for sulphur looks quite similar to the chain model, though the broken rings are merely a consequence of 'slicing' through the configuration. However this does illustrate quite clearly that the difference between chain and ring models in terms of the actual atomic positions, and hence of $S(Q)$, is very small. The relative merits of chain and ring models for sulphur will be discussed elsewhere.

4.2 *Comparison with other simulations*

It is difficult to make comparison with other simulations over the whole series of elements studied here. There have been many Monte Carlo or molecular dynamics simulations of the simple liquids, using 2-body potentials, and in most cases these agree quite well with the experimental data. We have learnt nothing particularly new in that respect, except in the sense of self-consistency of approach. For the weakly covalent liquids, as defined here, there have been very few simulations that agree quantitatively with the data. Those of Dzugutov *et al.* for lead[9] and bismuth[13] are probably the best in this sense, but they have concentrated on the form of the interatomic potentials required and the dynamics, not on local structural correlations. Of the rest the series of simulations by Hafner and co-workers is undoubtedly the most complete and reliable (see Ref. 14 and references therein). They have concentrated on the approach using pseudopotentials. While their models do not fit the data as well as those shown here, there are nevertheless considerable similarities between the major features of the 3-body correlations. For instance the bond angle distribution for arsenic is very similar[15] and their description of the structure of tellurium, 'entangled broken chain'[16], describes the structure we obtain perfectly. This confirms that, even though RMC does not use an interatomic potential, it does not generally produce physically unsensible results. The cases where RMC does not work well, that is where there is strong covalent bonding but not rigid molecules (such as selenium, sulphur and phosphorus), are also cases where it has so far proved impossible to derive suitable potentials[17].

The recently developed technique of *ab initio* molecular dynamics[18] offers some hope for understanding these more complex systems. Here a full quantum mechanical treatment is given to the bonding electrons, effectively producing a complete many-body potential. While such an approach has considerable possibilities there are still some problems to be overcome. Firstly the method is extremely computationally expensive so only small models (typically 64 atoms) have been studied. For systems with possible long chain structures (e.g. selenium) the boundary effects must be considerable. Secondly the choice of pseudopotentials to represent the core electrons can influence the results, and this choice is often empirical. Unfortunately the only two elemental liquids that have been studied in detail are carbon[19], for which no experimental data exist, and silicon[20] for which the data are poor. The results of the *ab initio* method have not therefore been quantitively tested, though the structure factor for silicon does agree well with the X-ray data[16] within the likely errors. It is worth noting that the bond angle distribution derived for silicon is very similar to that obtained from RMC modelling for germanium, and the 'fluctuation toward local tetrahedral order' so elegantly observed from electron density maps is precisely what has been described above.

5 CONCLUSIONS

The RMC method has been used to model the structures of a large number of elemental liquids. Detailed information, which is not obtainable directly from the structure factors or radial distribution functions, has been obtained on structural trends through the periodic table. These have been discussed in terms of the competition between close packing and covalency. We have made no attempt to specify, in terms of the interatomic potential or of electronic states, what is actually meant by stronger or weaker covalency; this has already been well discussed by Hafner[14]. We have only attempted to describe the trends in structural terms. Since RMC does not use a potential the structures produced cannot be considered to be in any kind of thermodynamic equilibrium. On the other hand simulation models based on a potential are in equilibrium but do not agree well with the experimental data. What is perhaps required is some combination of the two approaches, with both a potential and data being used to produce a model; this possibility is being investigated.

It is worth stressing here that all simulation methods have their particular advantages and disadvantages in the study of liquids. The RMC method only provides information on structure, not on dynamics, and so has restricted applicability. However we would emphasise that *quantitative* agreement with experimental data is important if *detailed* conclusions are to be drawn, particularly for some of the more subtle effects described here. We would also stress that direct interpretation of features in the experimental $S(Q)$ or $g(r)$ can be misleading; a proper structural model, obtained by one of the available techniques, is necessary if liquid structures are to be understood[4].

For the future it is clear that, in order to understand the subtle differences between

the structures of the many elemental liquids where three-body forces play a significant, but minor, role there is a requirement for significantly more accurate experimental data than are currently available. Since the differences between these and the 'simple' liquids are small the systematic errors in the measured structure factors must be correspondingly smaller. Further work is also required on the representation of many-body correlations. The function $b(\cos\theta)$ used here is simple but 'hides' many of the features shown in the more complex $g(r, \cos\theta)$. However even this function has only been subject to very qualitative interpretation. A promising extension of the use of spherical harmonic invariants is being made by Calvo[21] but other approaches are also needed.

Acknowledgements

We would like to thank Dr John Dore for providing us with his data on phosphorus, Dr R. Winter for data on caesium, Professor W. van der Lugt for data on lead and the alkali metals and Professor P. A. Egelstaff, Dr R. Winter and Dr W. S. Howells for data on sulphur. RLM thanks the Royal Society for their support for his research, without which the RMC method would not have been developed. L.P. thanks the Széchenyi Istvan Scholarship foundation for financial support during this work. I.B. thanks the Commission of the European Community for the provision of a scholarship under the TEMPUS program.

References

1. R. L. McGreevy and M. A. Howe, *Phys. Chem. Liq.*, **24**, 1 (1991).
2. R. L. McGreevy and L. Pusztai, *Mol. Simulation*, **1**, 359 (1988).
3. N. Metropolis, A. W. Rosenbluth, M. N. Rosenbluth, A. H. Teller and E. Teller, *J. Phys. Chem.*, **21**, 1087 (1953).
4. R. L. McGreevy, *J. Phys: Condensed Matter*, **3**, F9 (1991).
5. M. A. Howe, *Mol. Phys.*, **69**, 161 (199).
6. V. M. Nield, M. A. Howe and R. L. McGreevy, *J. Phys: Condensed Matter*, **3**, 7519 (1991).
7. L. Pusztai and R. L. McGreevy, *Phys. Chem. Liq.*, **24**, 119 (1991).
8. A. Baranyai, A. Geiger, P. R. Gartrell-Mills, K. Heinzinger, R. L. McGreevy, G. Pálinkás and I. Ruff, *J. Chem. Soc. Faraday Trans. II*, **83**, 1875 (1987).
9. M. Dzugutov, K.-E. Larsson and I. Ebbsjö, *Phys. Rev.*, **A38**, 3609 (1988).
10. C. N. Greaves, S. R. Elliott and E. A. Davis, *Adv. Phys.*, **28**, 49 (1979).
11. W. B. Streett and D. J. Tildesley, *Proc. R. Soc. A*, **348**, 485 (1976).
12. W. B. Streett and D. J. Tildesley, *Proc. R. Soc. A*, **335**, 239 (1977).
13. M. Dzugutov and U. Dahlborg, *Phys. Rev.*, **A40**, 4103 (1989).
14. J. Hafner, *J. Phys: Condensed Matter*, **3**, F23 (1991).
15. J. Hafner, *Phys. Rev. Lett.*, **62**, 784 (1989).
16. J. Hafner, *J. Phys: Condensed Matter*, **2**, 1271 (1990).
17. F. H. Stillinger, T. A. Weber and R. A. LaViolette, *J. Chem. Phys.*, **85**, 6460 (1986).
18. R. Car and M. Parrinello, *Phys. Rev. Lett.*, **55**, 2471 (1985).
19. G. Galli, R. M. Martin, R. Car and M. Parrinello, *Phys. Rev. Lett.*, **63**, 988 (1989).
20. I. Stich, R. Car and M. Parrinello, *Phys. Rev. Lett.*, **63**, 2240 (1989).
21. M. Calvo, *Mat. Sci. Engng.*, **A134**, 968 (1991).
t1. J.-P. Gabathuler, S. Steeb and P. Lamparter, *Z. Naturforsch.*, **34a**, 1305 (1979).
t2. J. L. Yarnell, M. J. Katz, R. G. Wenzel and S. H. Koenig, *Phys. Rev. A*, **7**, 2130 (1973).
t3. R. Bellisent, C. Bergman, R. Ceolin and J. P. Gaspard, *Phys. Rev. Lett.*, **59**, 661 (1987).
t4. W. Martin, W. Freyland, P. Lamparter and S. Steeb, *Phys. and Chem. Liq.*, **10**, 49 (1986).
t5. U. Dahlborg and M. Davidovic, *Phys. Chem. Liq.*, **15**, 243 (1986).
t6. A. H. Narten, R. Agrawal and S. J. Sandler, *Mol. Phys.*, **55**, 887 (1978).
t7. J. van Tricht, *Interuniversitair Reactor Instituut report IRI 132-84-12* (1984).
t8. K. S. Vahvaselka, *Phys. Scr.*, **24**, 59 (1981).
t9. M. J. Huijben and W. van der Lugt, *Acta Crystallogr. A*, **35**, 431 (1980).

t10. R. Winter, T. Bodensteiner, W. Gläser and F. Hensel, *Ber. Bunsen. Phys. Chem.*, **91**, 1327 (1987).
t11. O. J. Eder, E. Erdpresser, B. Kunsch, H. Stiller and M. Suda, *J. Phys. F: Metal Phys.*, **10**, 183 (1980).
t12. Y. Waseda and W. A. Miller, *Phil. Mag. B*, **38**, 21 (1978).
t13. C. Andreani, F. Cilloco and E. K. Osae, *Mol. Phys.*, **57**, 21 (1986).
t14. A. H. Narten, *J. Chem. Phys.*, **56**, 1185 (1972).
t15. P. S. Salmon, *J. Phys. F: Metal Phys.*, **18**, 2345 (1988).
t16. Y. Waseda and K. Suzuki, *Z. Phys. B*, **20**, 339 (1975).
t17. F. H. Wirth and R. B. Hallock, *Phys. Rev. B*, **35**, 89 (1987).
t18. L. Bosio, R. Cortes and C. Segaud, *J. Chem. Phys.*, **71**, 3595 (1979).
t19. Y. Waseda and S. Tamaki, *Phil. Mag.*, **36**, 1 (1977).
t20. C. van der Marel, W. Bras and W. van der Lugt, *Mol. Phys.*, **64**, 445 (1988).
t21. R. Bek, E. Wold and S. Steeb, *Z. Naturforsch*, **36a**, 150 (1981).
t22. R. W. Ohse (ed.), *Handbook of Thermodynamic and Transport properties of alkali metals Blackwell Scientific Publications.*
t23. G. T. Clayton and L. Heaton, *Phys. Rev.*, **121**, 649 (1961).
t24. H. Fredrikze, *Phys. Rev. A*, **36**, 2272 (1987).
t25. H. Olbrich, H. Ruppersburg, and S. Steeb, *Z. Naturforsch.*, **38a**, 1328 (1983).
t26. A. H. Narten, E. Johnson, and A. Habenschuss, *J. Chem. Phys.*, **73**, 1248 (1980).
t27. A. J. Greenfield, J. Wellendorf and N. Wiser, *Phys. Rev. A*, **4**, 1607 (1971).
t28. D. G. Henshaw, *Phys. Rev.*, **111**, 1470 (1958).
t29. L. A. De Graaf and B. Mozer, *J. Chem. Phys.*, **55**, 4967–4973 (1971).
t30. R. Granada and J. C. Dore, *Mol. Phys.*, **46**, 752 (1982).
t31. Van Wazer, *Phosphorus and its compounds* vol 1, 3rd ed. (Interscience).
t32. H. T. J. Reijers, W. van der Lugt, C. van Dijk and M.-L. Saboungi, *J. Phys: Condensed Matter*, **1**, 5529 (1989).
t33. Y. Waseda and M. Ohtani, *Z. Phys. B*, **21**, 229 (1975).
t34. V. M. Nield, R. L. McGreevy, D. A. Keen and M. A. Howe, '*Recent developments in the Physics of Fluids*': *Adam Hilger (UK)*. F211 (1992).
t35. Winter R, Szornel C., Pilgrim W.-C., Howells S., Egelstaff P. A. and Bodensteiner T., *J. Phys: Condensed Matter*, **2**, 8427 (1990).
t36. P. Lamparter, S. Steeb and W. Knoll, *Z. Naturforsch.*, **31a**, 90 (1976).
t37. Y. Waseda and K. Suzuki, *Phys. Status Solidi b*, **47**, 581 (1971).
t39. K. Suzuki, *Ber. Bunsen.*, **80**, 689 (1976).
t40. W. Martin, W. Freyland, P. Lamparter, and S. Steeb, *Phys. Chem. Liq.*, **10**, 49–60 (1980).
t43. S. Takeda, S. Tamaki and Y. Waseda, *J. Phys. Soc. Jpn*, **54**, 2552 (1985).
t44. A. Menelle, R. Bellisent and A. M. Flank, *Physica*, **156 & 157**, 174 (1989).
t45. H. Thurn and J. Ruska, *J. Non-Cryst. Sol.*, **22**, 331 (1976).
t46. S. Takeda, S. Tamaki and Y. Waseda, *J. Phys. Soc. Jpn*, **53**, 3830 (1984).
t47. S. Takeda, S. Harada, S. Tamaki and Y. Waseda, *J. Phys. Soc. Jpn*, **55**, 3437 (1986).
t48. N. C. Halder and C. N. J. Wagner (1966), *J. Chem. Phys.*, **45**, 482 (1966).
t49. S. Takeda, S. Tamaki, Y. Waseda and S. Harada, *J. Phys. Soc. Jpn*, **55**, 184 (1986).